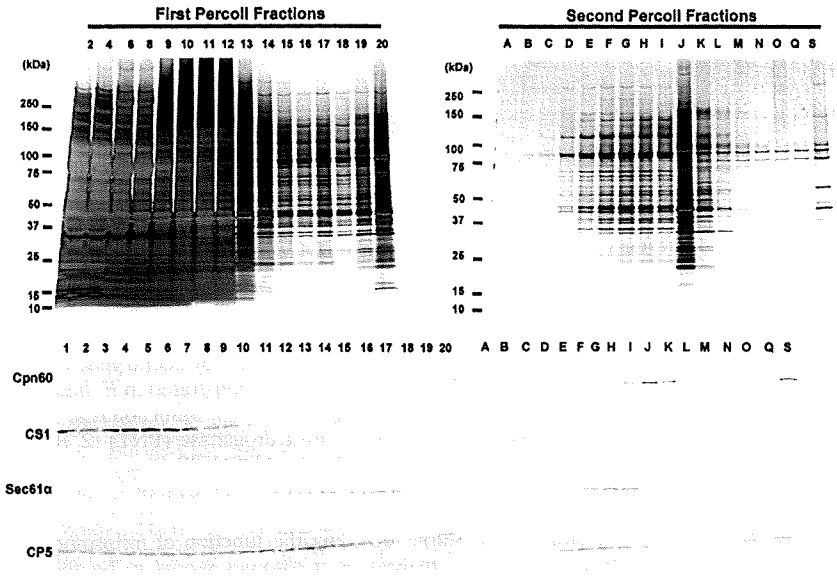

Fig. 1. Purification of mitosomes. Fractions derived from the first (fractions 1–20) and second (fractions A-S) discontinuous Percoll gradient centrifugation were electrophoresed on 5%–20% SDS/PAGE and subjected to immunoblot analyses using antibodies against well established organelle markers: Cpn60 (mitosome), cysteine synthase 1 (CS1; cytoplasm), Sec61α (endoplasmic reticulum), and CP5 (lysosome).

later). Three transporters and 7 metabolic enzymes were also identified. In addition, 7 proteins involved in membrane trafficking, including 4 Rab family GTPases, were detected. Furthermore, a weak homologue of Tom40 (expectation value of 0.13), a component of the transport complex of the outer membrane of the mitochondria, was identified. Three chaperones, Cpn60, Cpn10, mitochondrial Hsp70, and MCF, which were previously reported as *Entamoeba* mitosomal proteins (12–15), were also confirmed. Conversely, PNT and 2 proteins involved in the NIF system—NifS and NifU—were not detected. The proteome described here is likely to be partial, as only proteins enriched in fraction J were considered as mitosomal proteins, although Cpn60 was detected throughout fractions I through S in the second gradient (Fig. 1). The heterogeneity displayed by mitosomes in the immunofluorescence assay (described later) also indicates that other subfractions of mitosomes have likely been excluded from the list.

Verification of the Mitosomal Localization of the Identified Proteins. To confirm the cellular localization of these proteins, 21 randomly chosen putative mitosomal proteins and 4 known mitosomal proteins were examined by immunofluorescence assay in *E. histolytica* cell lines expressing HA-tagged proteins. Among the 25 proteins examined, 22 proteins—including MCF, mitochondrial Hsp70, and Cpn10—colocalized with the mitosomal marker Cpn60 (Fig. 2, Fig. S2, and Table S1). These results validated our proteomic approach for the identification of mitosomal proteins.

The distribution of each protein in mitosomes was not uniform. We often observed variations in the signal intensity between Cpn60 and other mitosomal proteins including mitochondrial Hsp70 and MCF (Fig. 2 *C* and *G* and Fig. S2 *C*, *G*, *K*, and *O*). These observations indicated that the composition of mitosomes is not homogeneous. The heterogeneity in the distribution of individual mitosomal proteins was not a result of the overexpression of the HA-tagged proteins, because endogenous and HA-tagged Cpn60 were well co-localized (Fig. 2 *I–L*).

Compartmentalization of the Sulfate Activation Pathway in Mitosomes. AS, APSK, and IPP were identified as dominant constituents of mitosomes by proteomic analysis. Immunofluorescence imaging of *E. histolytica* cell lines expressing HA-tagged AS, APSK, and IPP revealed small punctate signals throughout the cytoplasm, which co-localized well with Cpn60 (Fig. 2 *A–H* and Fig. S2 *A–D*). Furthermore, XP_655928, one of the 5 putative sodium/sulfate symporters identified in the *E. histolytica* genome (XP_649603, XP_654527, XP_654503, XP_655928, and XP_657578), colocalized with Cpn60, suggesting its involvement in the uptake and transport of sulfate into mitosomes (Fig. S2 *E–H*).

To further demonstrate the presence of a functional sulfate activation pathway compartmentalized to mitosomes, AS and APSK activities were measured in the Percoll gradient centrifugation fractions using $Na_2[^{35}S]O_4$. Both [^{35}S]-labeled adenosine-5′-phosphosulfate (APS) and 3′-phosphoadenosine-5′-phosphosulfate (PAPS) were detected (Fig. 3). PAPS was predominantly detected in fractions 19 and 20 of the first centrifugation and fractions I through K of the second centrifugation (Fig. 3). The distribution of the PAPS-forming activity was similar to Cpn60 (Fig. 1). In contrast, APS was detected in nearly all fractions (i.e., D-S) of the second centrifugation. This suggests that AS is not exclusively localized to mitosomes, despite its clear mitosomal localization observed by immunofluorescence analysis. Alternatively, APS synthesis may be partially catalyzed by an unidentified protein.

Identification of Metabolites of Activated Sulfate. To examine the fate of activated sulfate in *E. histolytica*, we incubated trophozoites in

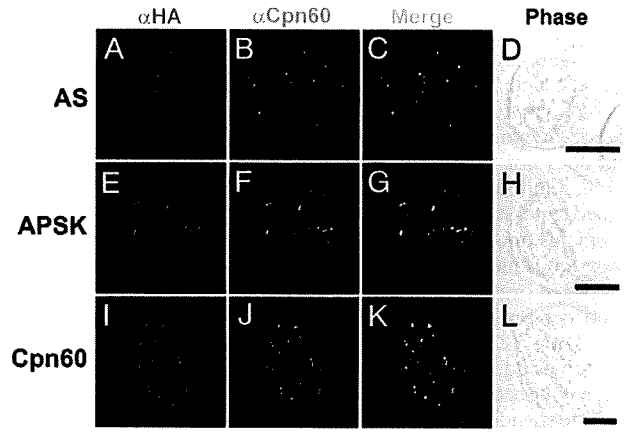

Fig. 2. Immunolocalization of representative mitosomal proteins. Colocalization of individual mitosomal proteins with the HA epitope (anti-HA antibody, red) and the authentic mitosomal protein marker Cpn60 (native Cpn60 antiserum, green) is shown (*A–H*). Colocalization of endogenous Cpn60 and exogenous HA-tagged Cpn60 is also shown (*I–L*). (Scale bars: 10 μm.)

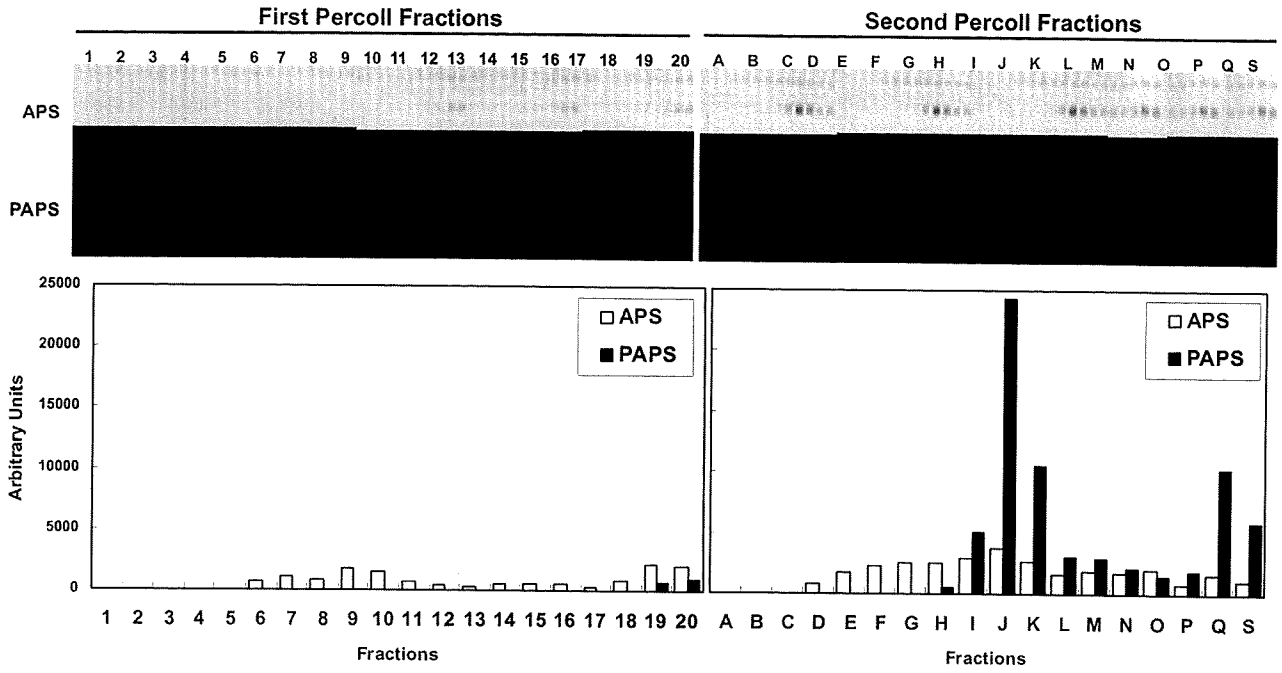

Fig. 3. Demonstration of AS and APSK activities. Mitosome-enriched fractions were tested for the ability to synthesize ^{35}S-labeled APS or PAPS (26). The reaction mixture for each sample totaled 12 μL and contained 39 mM $MgCl_2$, 64 mM ATP, 1.3 mM Na_2SO_4 (25 mCi/m mole), and 20 mM Tris/HCl (pH 8.0). The reaction was initiated by the addition of the freeze-thawed fraction (3 μL), carried out for 2 h at 25 °C, and terminated by the addition of 88 μL methanol. Ten-microliter samples were analyzed by PEI-cellulose TLC to determine ^{35}S-labeled APS or PAPS as previously described (27). The amount of each product was quantified by densitometric analysis using an image analyzer (Fuji) and the results are expressed in arbitrary units.

BI-S-33 medium containing $Na_2[^{35}S]O_4$ for up to 2 h, or labeled for 1 h and chased for up to 24 h. The cell lysate was separated into methanol-soluble and insoluble fractions. Labeled [^{35}S] was detected predominantly in the methanol-soluble fraction. At least 5 polar lipids, separated on a silica HPTLC plate in 25:65:10 (vol/vol/vol) methanol/chloroform/acetic acid (Fig. 4), accounted for most of the [^{35}S] detected (81.6% ± 6.2% at 1 h pulse). These lipids were distinct from commonly observed phospholipid species (phosphatidylethanolamine, phosphatidylserine, phosphatidylinositol, and phosphatidylcholine). These data indicate that activated sulfate is mainly used to synthesize sulfur-containing polar lipids.

Phylogenetic Analysis of the Sulfate Activation Pathway. To investigate the origin of sulfate activation in *E. histolytica*, phylogenetic analyses of the proteins involved in the pathway and established mitosomal chaperones were conducted. The origins of AS, APSK, IPP, sodium/sulfate symporter, Cpn60, and mitochondrial Hsp70 were not identical. *E. histolytica* AS showed strong affinity to AS from δ-proteobacteria (Fig. 5), whereas *E. histolytica* IPP clustered with IPP from other eukaryotes (Fig. S4). *E. histolytica* APSK was closely related to δ-proteobacteria, α-proteobacteria, and *Dictyostelium discoideum* (with low bootstrap values), and *E. histolytica* sodium/sulfate symporters clustered with a limited group of eukaryotes (diatoms and green algae) and bacteria, although their exact origins were not clearly resolved (Fig. S3 and Fig. S5). In contrast, *E. histolytica* Cpn60 and mitochondrial Hsp70 showed monophyly with the α-proteobacteria (8, 11, 22). The data indicate the phylogenetically mosaic nature of mitosomes in *E. histolytica*.

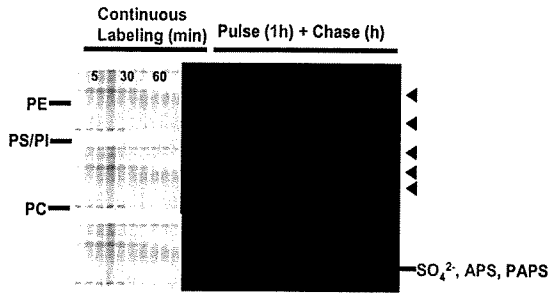

Fig. 4. Incorporation of [^{35}S]-labeled sulfate into polar lipids. ^{35}S was incorporated into at least 5 polar lipids (arrowheads), which were distinct from commonly observed phospholipid species. PE, phosphatidylethanolamine; PS, phosphatidylserine; PI, phosphatidylinositol; PC, phosphatidylcholine.

Discussion

Although the diversity in structure and function of mitochondrion-related organelles have been demonstrated in a wide range of organisms, *E. histolytica* remains as one of the anaerobic/microaerophilic eukaryotes, in which the function of the mitochondrion-related organelle remains unknown. In this study, we have provided biochemical and microscopic evidence demonstrating that sulfate activation, which generally occurs in the cytoplasm and plastids in eukaryotes, is the major function of mitosomes in *E. histolytica*.

Genes encoding for all of the major components necessary for sulfate activation and transport of substrates and products across the mitosomal membrane are identifiable in the genome (Fig. 6). Sodium/sulfate symporter, which is necessary for the uptake of sulfate into mitosomes, was identified. ATP that is necessary for the activation of sulfate by both AS and APSK, and the quality control of heat-sensitive AS by chaperones, is incorporated via MCF to mitosomes with a concomitant cytosolic export of ADP or AMP. *E. histolytica* MCF transports both ADP and AMP to the cytosol for the incorporation of ATP to mitosomes (14). In other organisms, PAPS transporter (PAPST), which transports PAPS and AMP in opposite directions, is required for shuttling PAPS between the

EVOLUTION

Fig. 5. Phylogenetic analysis of AS. The best maximum likelihood (*ML*) tree of AS inferred by the JTT model taking across-site rate heterogeneity into consideration. The α-value of the Γ-shaped parameter used in the analysis of AS was 0.50723. Bootstrap proportion (*BP*) values are attached to the internal branches. Branches with less than 50% BP support are unmarked. BP values are calculated by ML, distance matrix (*DM*), and maximum parsimony (*MP*) methods. One hundred and 1,000 resamplings were performed for ML and DM and MP analyses, respectively. The length of each branch is proportional to the estimated number of substitution. With 67 taxa, 302 aligned amino acid sites were used for analysis, corresponding to residues 55 to 103, 117 to 131, 135 to 147, 151 to 178, 182 to 196, 200 to 226, 231 to 262, 264 to 325m and 333 to 399 of the *E. histolytica* sequence.

organelle and the cytosol (28). Although the *E. histolytica* genome contains a gene encoding for putative PAPST (XP_654175; expectation value, 4.2^{-14}) (29, 30), we failed to demonstrate the mitosomal localization of the protein (PAPST; Fig. S6). In addition, a putative phosphate transporter (XP_654379; expectation value, 1.23^{-61}) (31) also failed to localize to mitosomes (PHT; Fig. S6). Thus, the identity of the presumptive PAPS and phosphate transporters in *E. histolytica* mitosomes remains unknown. Generally, PAPS is used in 2 different pathways. In one route, the sulfate moiety of PAPS is transferred to various acceptors to yield mucopolysaccharides, sulfolipids, and sulfoproteins by sulfotransferases. Alternatively, sulfate is reduced and assimilated into cysteine (32, 33). The *E. histolytica* genome contains 11 potential genes encoding for sulfotransferases, but lacks the enzymes for sulfate reduction (34, 35). Therefore, together with the results of $[^{35}S]O_4$ metabolic labeling (Fig. 4), it is conceivable to assume that PAPS predominantly serves as the sulfo-donor of sulfotransferases to synthesize sulfur-containing lipids. Two of the most highly expressed sulfotransferases (SULT1, XP_654200, expectation value, 1^{-12}; SULT2, XP_654101, expectation value, 1^{-13}) were distributed to the cytoplasm (SULT1 and SULT2; Fig. S6), suggesting that sulfo-transfer reactions occur in the cytosol, and thus reinforcing the premise that PAPS needs to be exported from mitosomes. Further characterization of these sulfur-containing lipid species in *E. histolytica* is necessary to understand the physiological significance of the compartmentalized sulfate activation in mitosomes of this organism.

As sulfate activation in eukaryotes generally occurs in the cytoplasm and plastids (36, 37), our finding has raised an important question on whether compartmentalization of sulfate activation in mitosomes is unique to *E. histolytica*. The acquisition and compart-

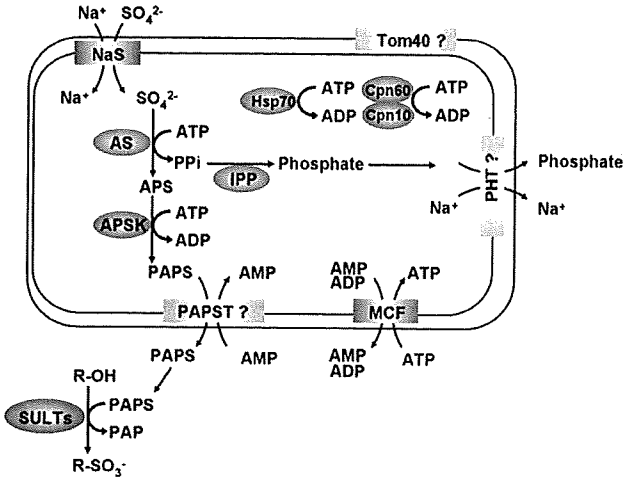

Fig. 6. A compartmentalized sulfate activation pathway in *E. histolytica* mitosomes. The mitosome proteins whose localization was confirmed by immunofluorescence assay are shown in red, whereas the putative transporters are shown in gray. PHT, phosphate transporter; SULT, sulfotransferase. Two of the most highly expressed sulfotransferases were demonstrated to be localized to the cytoplasm (Fig. S6).

mentalization of the enzymes involved in sulfate activation may have occurred exclusively in *Entamoeba* among the anaerobic/microaerophilic organisms possessing mitochondrion-related organelles. *T. vaginalis*, *G. intestinalis*, and *C. parvum* apparently lack genes encoding for the enzymes. *Encephalitozoon cuniculi*, one of the microsporidia, has the gene for IPP (Fig. S4), but lacks genes encoding for AS and APSK. Although the genome and EST databases are not complete for *M. balamuthi* and *N. patriciarum*, none of *AS*, *APSK*, and *IPP* genes was found so far. It is worth examining if genes involved in sulfate activation are present in *M. balamuthi* because the 2 species share the NIF system for FeS cluster biosynthesis (22). There is only one eukaryote, other than *E. histolytica*, that possesses sulfate activation in the mitochondria. In *Euglena gracilis*, the enzymatic activities involved in sulfate activation and reduction have been detected in the mitochondria (36, 38, 39). The origin of *E. gracilis* AS, however, is presumed to be the secondary green algal plastid and not the δ-proteobacteria (36), whereas *E. gracilis* IPP is thought to be derived from bacteria and not an ancestral eukaryote (Fig. S4). These results suggest that the origins of *E. gracilis* mitochondria are distinct from those of *E. histolytica* mitosomes. Based on the fact that the 4 *E. histolytica* proteins involved in sulfate transport and activation have origins distinct from α-proteobacterium, we propose a hypothesis whereby AS, APSK, and sodium/sulfate symporter were acquired by the ancestor of *Entamoeba* from δ-proteobacterium (and other bacteria) by lateral gene transfer (40). We examined whether AS and APSK were found in an operon in δ-proteobacteria, which would support the hypothesis whereby both AS and APSK of δ-proteobacterial origin were transferred to the ancestor of *Entamoeba*. However, this is not a case in at least 2 representative species (*Desulfotalea psychrophila* and *Desulfovibrio vulgaris*).

Various diverse or sometimes shared characteristics are reported in other eukaryotes possessing either hydrogenosomes or mitosomes. These include hydrogenase and pyruvate:ferredoxin oxidoreductase for ATP generation in hydrogenosomes; NADH dehydrogenase part of mitochondrial complex I in *T. vaginalis*, *N. ovalis*, and *Blastocystis*; TCA cycle enzymes in *M. balamuthi*, *Blastocystis*, *N. patriciarum*, *and N. ovalis*; glycine cleavage complex in *M. balamuthi*, *T. vaginalis*, and *Blastocystis*; and alternative oxidase in *Blastocystis* and *C. parvum* (1). Cpn60 and the ISC system were thought to be shared characteristics of hydrogenosomes and mitosomes in anaerobic/microaerophilic eukaryotes (1). However, *E. histolytica* and *M. balamuthi* possess only the NIF system instead of the ISC system (22, 24). In the mitosomal proteome, neither NifS nor NifU was identified in the mitosome-enriched fraction. We previously reported that NifS and NifU, both of which lack a mitochondrion-targeting signal, were fractionated on an anion exchange chromatography from the soluble fraction obtained by 0.45-μm filtration and 45,000 × *g* ultracentrifugation of amoebic lysate, suggesting the predominantly cytoplasmic localization of the NIF system in *E. histolytica* (24). Similarly, both NifS and NifU in *M. balamuthi* lack a mitochondria targeting signal (22). These data suggest that FeS cluster biosynthesis in *E. histolytica* and *M. balamuthi* are mainly, if not exclusively, localized to the cytosol (22, 24). However, it remains unknown whether the *E. histolytica* mitosomes also partially contain the NIF system.

The targeting mechanisms to the *E. histolytica* mitosomes remain unsolved and need further investigation. Although *Entamoeba* PNT was presumed to be imported into mitosomes based on the resemblance of its amino-terminal portion rich in hydroxylated and basic amino acids to the canonical mitochondrial targeting peptide (2), our proteomic and immunofluorescence studies clearly showed that PNT is not imported to mitosomes, but is distributed to vesicles and vacuoles (Fig. S7). Commonly available prediction programs such as Mitoprot (41) and PSORT II (42) were unable to correctly predict the mitosomal localization of proteins whose localization was verified by immunofluorescence assay. Similarly, the remaining putative mitosomal proteins have no predictable mitochondrial targeting signal. As described earlier, our mitosomal proteome contained a weak homologue of Tom40 (expectation value, 0.13). Thus, there is a need to verify the identity of this potential Tom40 and the existence of the Tom complex in *E. histolytica*. In other anaerobic eukaryotes, protein import machinery to the mitochondrion-related organelles appears to be conserved (43, 44), and the mitosomal targeting signal from *G. lamblia* and the hydrogenosome targeting signal from *T. vaginalis* were interchangeable (45). On the contrary, cryptic mitochondrial targeting signals have also been discovered in *G. lamblia*, T. vaginalis, and microsporidian species, and unique aspects of mitochondrial processing peptidases have been reported in *G. lamblia* (1, 46). Together, the machinery and mechanisms of protein import into mitosomes require further investigation.

In summary, we have shown that *E. histolytica* mitosomes are a mitochondrion-related organelle that is highly divergent and represents a mosaic organelle consisting of proteins derived from α-proteobacteria, δ-proteobacteria, and eukaryotes. It is primarily involved in sulfate activation. This study should shed light on the diversification of mitochondrion-related organelles in eukaryotic evolution.

Materials and Methods

Mitosome Purification. Approximately 0.5–1 × 10^8 trophozoites of *E. histolytica* strain HM-1:IMSS cl6 (47), cultivated axenically in Diamond BI-S-33 medium (48), were resuspended in 1 mL of homogenate buffer [250 mM sucrose, protease inhibitor mixture (Roche), 300 μM E-64, 10 mM Mops-KOH (pH 7.4)], and homogenized with a Dounce homogenizer. Unbroken cells, nuclei, and large vacuoles were removed by centrifugation at 5,000 × *g* at 4 °C for 10 min, and the supernatant was gently layered onto 3 mL of homogenization buffer containing 30% (vol/vol) Percoll. After centrifugation at 120,000 × *g* at 4 °C for 1 h, 200 μL fractions were collected from top to bottom (fractions 1–20). Fractions 19 and 20 (density >1.054) were collected, mixed, and applied onto 2 mL of homogenization buffer containing 70% (vol/vol) Percoll. The gradient was subsequently overlaid with 1 mL of the homogenization buffer containing 15% (vol/vol) Percoll. After centrifugation at 120,000 × *g* at 4 °C for 1 h, 200 μL of fractions were collected from top to bottom (fractions A-S; Fig. S1).

Immunoblot Analysis. Fractions prepared as previously mentioned were mixed with 4× SDS/PAGE sample buffer. Samples were boiled at 95 °C for 5 min followed by centrifugation at 13,000 × *g* at 4 °C for 20 min to remove the Percoll. The fractions were analyzed by SDS/PAGE, silver stained, and immunoblot analysis as

previously described (49). The dilution of the primary antibodies was 1:1,000 for anti-Cpn60 and anti-cysteine synthase 1 antiserum, and 1:100 for anti-CP5 and anti-Sec61α antiserum (50, 51).

Production of *E. histolytica* Lines Expressing Epitope-Tagged Mitosomal Proteins. Plasmids for the production of amoeba lines expressing engineered mitosomal proteins containing 3 tandem HA-epitopes were constructed essentially as previously described (52). Lipofection of trophozoites and selection of transformants were also performed as previously described (53).

Indirect Immunofluorescence Assay. Indirect immunofluorescence assay was performed as previously described (49) with some modifications. Briefly, the amoebae were washed and fixed with acetone/methanol (1:1) for 10 min. After washing with PBS solution, cells were permeabilized with 0.3% Triton X-100 for 15 min and reacted with primary antibody diluted at 1:500 (anti-Cpn60 antiserum) and 1:1,000 (anti-HA monoclonal antibody) in PBS solution. The samples were then reacted with Alexa Fluor 488- or 568-conjugated anti-rabbit or anti-mouse secondary antibody (1:1,000) for 1 h. The samples were examined as previously described (49).

Metabolic Labeling. Approximately 10^6 trophozoites were labeled with [^{35}S]-labeled sulfate (25 mCi/m mole) in 0.5 mL of the Diamond BI-S-33 medium either continuously for 5 to 120 min or labeled for 1 h and chased for 1 to 24 h (54). Cells were collected and lipids were extracted with 0.5 mL of methanol and separated on a silica high-performance thin-layer chromatography plate in 25:65:10 (vol/vol/vol) methanol/chloroform/acetic acid. Dried thin-layer chromatography plates were analyzed by autoradiography.

ACKNOWLEDGMENTS. We thank Dr. Takeshi Makiuchi for discussions of phylogenetic analysis. We thank Yoko Yamada, Kyoko Masuda, Kayoko Hashimoto, and Rumiko Kosugi for technical assistance. We thank Jorge Tovar, Royal Holloway University of London, for anti-Cpn60 antibody for an initial analysis of Cpn60. We also thank Rosana Sánchez-López, UNAM, Cuernavaca, Mexico, for anti-Sec61α antiserum. This work was supported by Creative Scientific Research Grant 18GS0314 from the Japanese Ministry of Education, Science, Culture, Sports, and Technology (to T.N.); Grant-in-Aid for Scientific Research (18GS0314, 18050006, 18073001) from the Ministry of Education, Culture, Sports, Science and Technology of Japan; a grant for research on emerging and re-emerging infectious diseases from the Ministry of Health, Labour and Welfare of Japan; and a grant for research to promote the development of anti-AIDS pharmaceuticals from the Japan Health Sciences Foundation (to T.N.).

1. van der Giezen M (2009) Hydrogenosomes and mitosomes: conservation and evolution of functions. *J Eukaryot Microbiol* 56:221–231.
2. Aguilera P, Barry T, Tovar J (2008) *Entamoeba histolytica* mitosomes: organelles in search of a function. *Exp Parasitol* 118:10–16.
3. Lindmark DG, Muller M (1973) Hydrogenosome, a cytoplasmic organelle of the anaerobic flagellate *Tritrichomonas foetus*, and its role in pyruvate metabolism. *J Biol Chem* 248:7724–7728.
4. Hrdy I, et al. (2004) *Trichomonas* hydrogenosomes contain the NADH dehydrogenase module of mitochondrial complex I. *Nature* 432:618–622.
5. Yarlett N, Orpin CG, Munn EA, Yarlett NC, Greenwood CA (1986) Hydrogenosomes in the rumen fungus *Neocallimastix patriciarum*. *Biochem J* 236:729–739.
6. van der Giezen M, et al. (2003) Fungal hydrogenosomes contain mitochondrial heat-shock proteins. *Mol Biol Evol* 20:1051–1061.
7. Hackstein JH, Tjaden J, Huynen M Mitochondria, hydrogenosomes and mitosomes: products of evolutionary tinkering! *Curr Genet* 50:225–245, 2006.
8. Clark CG, Roger AJ (1995) Direct evidence for secondary loss of mitochondria in *Entamoeba histolytica*. *Proc Natl Acad Sci USA* 92:6518–6521.
9. Mai, Z, et al. (1999) Hsp60 is targeted to a cryptic mitochondrion-derived organelle ("crypton") in the microaerophilic protozoan parasite *Entamoeba histolytica*. *Mol Cell Biol* 19:2198–2205.
10. Tovar J, Fischer A, Clark CG (1999) The mitosome, a novel organelle related to mitochondria in the amitochondrial parasite *Entamoeba histolytica*. *Mol Microbiol* 32:1013–1021.
11. Bakatselou C, Kidgell C, Clark CC (2000) A mitochondrial-type hsp70 gene of *Entamoeba histolytica*. *Mol Biochem Parasitol* 110:177–182.
12. Leon-Avila G, Tovar J (2004) Mitosomes of *Entamoeba histolytica* are abundant mitochondrion-related remnant organelles that lack a detectable organellar genome. *Microbiology* 150:1245–1250.
13. van der Giezen M, Leon-Avila G, Tovar J (2005) Characterization of chaperonin 10 (Cpn10) from the intestinal human pathogen *Entamoeba histolytica*. *Microbiology* 151:3107–3115.
14. Chan KW, et al. (2005) A novel ADP/ATP transporter in the mitosome of the microaerophilic human parasite *Entamoeba histolytica*. *Curr Biol* 15:737–742.
15. Tovar J, Cox SS, van der Giezen M (2007) A mitosome purification protocol based on percoll density gradients and its use in validating the mitosomal nature of *Entamoeba histolytica* mitochondrial Hsp70. *Methods Mol Biol* 390:167–177.
16. Tovar J, et al. (2003) Mitochondrial remnant organelles of *Giardia* function in iron-sulphur protein maturation. *Nature* 426:172–176.
17. Dolezal P, et al. (2005) *Giardia* mitosomes and trichomonad hydrogenosomes share a common mode of protein targeting. *Proc Natl Acad Sci USA* 102:10924–10929.
18. Burri L, Williams BA, Bursac D, Lithgow T, Keeling PJ (2006) Microsporidian mitosomes retain elements of the general mitochondrial targeting system. *Proc Natl Acad Sci USA* 103:15916–15920.
19. Goldberg AV, et al. (2008) Localization and functionality of microsporidian iron-sulphur cluster assembly proteins. *Nature* 452:624–628.
20. Tsaousis AD, et al. (2008) A novel route for ATP acquisition by the remnant mitochondria of. *Encephalitozoon cuniculi*. *Nature* 453:553–556.
21. Henriquez FL, Richards TA, Roberts F, McLeod R, Roberts CW (2005) The unusual mitochondrial compartment of *Cryptosporidium parvum*. *Trends Parasitol* 21:68–74.
22. Gill EE, et al. (2007) Novel mitochondrion-related organelles in the anaerobic amoeba *Mastigamoeba balamuthi*. *Mol Microbiol* 66:1306–1320.
23. Stechmann A, et al. (2008) Organelles in *Blastocystis* that blur the distinction between mitochondria and hydrogenosomes. *Curr Biol* 18:580–585.
24. Ali V, Shigeta Y, Tokumoto U, Takahashi Y, Nozaki T (2004) An intestinal parasitic protist, *Entamoeba histolytica*, possesses a non-redundant nitrogen fixation-like system for iron-sulfur cluster assembly under anaerobic conditions *J Biol Chem* 279:16863–16874.
25. Nozaki T, et al. (1998) Cloning and bacterial expression of adenosine-5′-triphosphate sulfurylase from the enteric protozoan parasite *Entamoeba histolytica*. *Biochim Biophys Acta* 1429:284–291.
26. Leyh TS, Taylor JC, Markham GD (1988) The sulfate activation locus of *Escherichia coli* K12: cloning, genetic, and enzymatic characterization. *J Biol Chem* 263:2409–2416.
27. Yanagisawa K, et al. (1998) cDNA cloning, expression, and characterization of the human bifunctional ATP sulfurylase/adenosine 5′-phosphosulfate kinase enzyme. *Biosci Biotechnol Biochem* 62:1037–1040.
28. Capasso JM, Hirschberg CB (1984) Mechanisms of glycosylation and sulfation in the Golgi apparatus: evidence for nucleotide sugar/nucleoside monophosphate and nucleotide sulfate/nucleoside monophosphate antiports in the Golgi apparatus membrane. *Proc Natl Acad Sci USA* 81:7051–7055.
29. Kamiyama S, et al. (2003) Molecular cloning and identification of 3′-phosphoadenosine 5′-phosphosulfate transporter. *J Biol Chem* 278:25958–25963.
30. Kamiyama S, et al. (2006) Molecular cloning and characterization of a novel 3′-phosphoadenosine 5′-phosphosulfate transporter, PAPST2. *J Biol Chem* 281:10945–10953.
31. Guo B, Irigoyen S, Fowler TB, Versaw WK (2008) Differential expression and phylogenetic analysis suggest specialization of plastid-localized members of the PHT4 phosphate transporter family for photosynthetic and heterotrophic tissues. *Plant Signal Behav* 3:784–790.
32. Strott CA (2002) Sulfonation and molecular action. *Endocr Rev* 23:703–732.
33. Negishi M, et al. (2001) Structure and function of sulfotransferases. *Arch Biochem Biophys* 390:149–157.
34. Clark CG, et al. (2007) Structure and content of the *Entamoeba histolytica* genome. *Adv Parasitol* 65:51–190.
35. Ali V, Nozaki T (2007) Current therapeutics, their problems, and sulfur-containing-amino-acid metabolism as a novel target against infections by "amitochondriate" protozoan parasites. *Clin Microbiol Rev* 20:164–187.
36. Patron NJ, Durnford DG, Kopriva S (2008) Sulfate assimilation in eukaryotes: fusions, relocations and lateral transfers. *BMC Evol Biol* 8:1–14.
37. Bradley ME, Rest JS, Li WH, Schwartz NB (2009) Sulfate activation enzymes: phylogeny and association with pyrophosphatase. *J Mol Evol* 68:1–13.
38. Brunold C, Schiff JA (1976) Studies of sulfate utilization of algae: 15. Enzymes of assimilatory sulfate reduction in *Euglena* and their cellular localization. *Plant Physiol* 57:430–436.
39. Saidha T, Na SQ, Li JY, Schiff JA (1988) A sulphate metabolizing centre in *Euglena* mitochondria. *Biochem J* 253:533–539.
40. Loftus B, et al. (2005) The genome of the protist parasite. *Entamoeba histolytica Nature* 433:865–868.
41. Claros MG, Vincens P (1996) Computational method to predict mitochondrially imported proteins and their targeting sequences. *Eur J Biochem* 241:779–786.
42. Nakai K, Horton P (1999) PSORT: a program for detecting sorting signals in proteins and predicting their subcellular localization. *Trends Biochem Sci* 24:34–36.
43. Dolezal, et al. (2006) Evolution of the molecular machines for protein import into mitochondria. *Science* 313:314–318.
44. Dagley MJ, et al. (2009) The protein import channel in the outer mitosomal membrane of *Giardia intestinalis*. *Mol Biol Evol* 26:1941–1947.
45. Dolezal P, et al. (2005) *Giardia* mitosomes and trichomonad hydrogenosomes share a common mode of protein targeting. *Proc Natl Acad Sci USA* 102:10924–10929.
46. Smid O, et al. (2008) Reductive evolution of the mitochondrial processing peptidases of the unicellular parasites *Trichomonas vaginalis* and *Giardia intestinalis*. *PLoS Pathog* 4: e1000243.
47. Diamond LS, Mattern CF, Bartgis IL (1972) Viruses of *Entamoeba histolytica*. I. Identification of transmissible virus-like agents. *J Virol* 9:326–341.
48. Diamond LS, Harlow DR, Cunnick CC (1978) A new medium for the axenic cultivation of *Entamoeba histolytica* and other. *Entamoeba Trans R Soc Trop Med Hyg* 72:431–432.
49. Nakada-Tsukui K, Saito-Nakano Y, Ali V, Nozaki T (2005) A retromerlike complex is a novel Rab7 effector that is involved in the transport of the virulence factor cysteine protease in the enteric protozoan parasite *Entamoeba histolytica*. *Mol Biol Cell* 16:5294–5303.
50. Nozaki T, et al. (1998) Molecular cloning and characterization of the genes encoding two isoforms of cysteine synthase in the enteric protozoan parasite *Entamoeba histolytica*. *Mol Biochem Parasitol* 97:33–44.
51. Mitra BN, Saito-Nakano Y, Nakada-Tsukui K, Sato D, Nozaki T (2007) Rab11B small GTPase regulates secretion of cysteine proteases in the enteric protozoan parasite *Entamoeba histolytica*. *Cell Microbiol* 9:2112–2125.
52. Saito-Nakano Y, Yasuda T, Nakada-Tsukui K, Leippe M, Nozaki T (2004) Rab5-associated vacuoles play a unique role in phagocytosis of the enteric protozoan parasite *Entamoeba histolytica*. *J Biol Chem* 279:49497–49507.
53. Nozaki T, et al. (1999) Characterization of the gene encoding serine acetyltransferase, a regulated enzyme of cysteine biosynthesis from the protist parasites *Entamoeba histolytica* and *Entamoeba dispar*. Regulation and possible function of the cysteine biosynthetic pathway in *Entamoeba*. *J Biol Chem* 274:32445–32452.
54. Bakker-Grunwald T, Geilhorn B (1992) Sulfate metabolism in *Entamoeba histolytica*. *Mol Biochem Parasitol* 53:71–78.

G Model
ANTAGE-3125; No. of Pages 6
ARTICLE IN PRESS

International Journal of Antimicrobial Agents xxx (2009) xxx–xxx

Contents lists available at ScienceDirect

International Journal of Antimicrobial Agents

journal homepage: http://www.elsevier.com/locate/ijantimicag

Cytotoxic effect of amide derivatives of trifluoromethionine against the enteric protozoan parasite *Entamoeba histolytica*

Dan Sato[a,b], Seiki Kobayashi[c], Hiroyuki Yasui[d], Norio Shibata[d], Takeshi Toru[d], Masaichi Yamamoto[e], Gensuke Tokoro[e], Vahab Ali[f,1], Tomoyoshi Soga[a], Tsutomu Takeuchi[c], Makoto Suematsu[b], Tomoyoshi Nozaki[f,g,*]

[a] *Institute for Advanced Biosciences, Keio University, Tsuruoka, Yamagata 997-0052, Japan*
[b] *Center for Integrated Medical Research, School of Medicine, Keio University, Shinjuku, Tokyo 160-8582, Japan*
[c] *Department of Parasitology, School of Medicine, Keio University, Shinjuku, Tokyo 160-8582, Japan*
[d] *Department of Frontier Materials, Graduate School of Engineering, Nagare College, Nagoya Institute of Technology, Nagoya 466-8555, Japan*
[e] *aRigen Pharmaceuticals Incorporated, 7-3-37/3F, Akasaka, Minato-ku, Tokyo 107-0052, Japan*
[f] *Department of Parasitology, Gunma University Graduate School of Medicine, Maebashi, Gunma, Japan*
[g] *Department of Parasitology, National Institute of Infectious Diseases, Shinjuku, Tokyo 162-8640, Japan*

ARTICLE INFO

Article history:
Received 23 April 2009
Accepted 3 August 2009

Keywords:
Drug discovery
Sulphur-containing amino acid metabolism
Methionine γ-lyase
Protozoan parasite

ABSTRACT

Amoebiasis, caused by infection with the enteric protist *Entamoeba histolytica*, is one of the major parasitic diseases. Although metronidazole and its derivatives are currently employed in therapy, the paucity of effective drugs and potential clinical resistance necessitate the development of a novel drug. Trifluoromethionine (TFM) is a promising lead compound for antiamoebic drugs. To potentiate the antiamoebic effect of TFM, we synthesised various amide derivatives of TFM and evaluated their cytotoxicity. The amide derivatives of TFM were observed to have a superior cytotoxic effect compared with TFM and metronidazole against *E. histolytica* in vitro. Although TFM showed cytotoxicity following degradation by methionine γ-lyase, the derivatives were degraded by the enzyme less efficiently compared with TFM. We further demonstrated that a representative derivative was hydrolysed by the amoebic cell lysate to first yield TFM, followed by degradation similar to TFM. Hydrolysis was partially inhibited by protease inhibitors. A single subcutaneous or oral administration of TFM and its amide derivatives also effectively prevented the formation of amoebic liver abscess in a rodent model. These data demonstrate the improved effectiveness of TFM derivatives against *E. histolytica* infection and elucidate the mechanisms underlining the mode of action of these compounds.

1. Introduction

Amoebiasis is an infectious disease caused by the enteric protozoan parasite *Entamoeba histolytica* and is the second leading cause of death from parasitic diseases after malaria. Only metronidazole and related compounds are commonly used against invasive intestinal and extraintestinal amoebiasis [1,2]. Although clinical resistance against metronidazole has not yet been demonstrated, sporadic cases of treatment failure have been reported [1]. In addition, it has been shown that this parasite easily adapts to therapeutic levels of metronidazole in vitro [3]. Resistance to metronidazole is also acquired easily by many bacterial species as well as *Giardia intestinalis* and *Trichomonas vaginalis* [1]. Therefore, the development of a novel antiamoebic drug is urgently required.

Pathways present exclusively in microorganisms but missing in humans may potentially represent a rational target for drug development. *Entamoeba histolytica* has several unique metabolic features. It lacks both the forward and reverse trans-sulphuration pathways that convert methionine to cysteine via cystathionine or vice versa, whilst it possesses L-methionine γ-lyase (MGL) (EC. 4.4.1.11) to decompose methionine, homocysteine and cysteine and produces ammonia, α-keto acid and volatile thiols [4]. MGL is present in only limited lineages of bacteria, parasitic protozoa and plants but is absent in mammals (see in [5]). In *E. histolytica*, two isoenzymes of MGL (MGL1 and MGL2) with distinct substrate specificities have been identified [5].

Trifluoromethionine (TFM), also know as *S*-trifluoromethyl-L-homocysteine, a fluorinated analogue of methionine, has been

* Corresponding author. Present address: Department of Parasitology, National Institute of Infectious Diseases, 1-23-1 Toyama, Shinjuku, Tokyo 162-8640, Japan. Tel.: +81 3 5285 1111x2600; fax: +81 3 5285 1219.
E-mail address: nozaki@nih.go.jp (T. Nozaki).
[1] Present address: Department of Biochemistry, Rajendra Memorial Research Institute of Medical Sciences, Agam Kuan, Patna 800007, India.

0924-8579/$ – see front matter © 2009 Elsevier B.V. and the International Society of Chemotherapy. All rights reserved.
doi:10.1016/j.ijantimicag.2009.08.016

shown to be highly toxic to bacteria, *Porphyromonas gingivalis*, *T. vaginalis* and *E. histolytica* in vitro [6–9]. It was also reported to treat infections by *P. gingivalis* and *T. vaginalis* in a rodent model [7,8]. In the present study, the in vitro and in vivo efficacy of TFM and its derivatives were examined to gain insight into the structure–activity relationship and to determine the mechanism underlying their mode of action.

2. Materials and methods

2.1. Chemical synthesis of trifluoromethionine and its derivatives

The synthetic scheme and structure of TFM and its analogues are shown in Supplementary Fig. 1.

2.2. Parasites and cultivation

Trophozoites of *E. histolytica* HM-1:IMSS cl6 were cultured axenically in BIS medium at 35.5 °C as described previously [10].

2.3. In vitro cytotoxicity assay of trifluoromethionine derivatives against Entamoeba histolytica trophozoites and Chinese hamster ovary (CHO) cells

Approximately 5×10^3 amoebae in 280 μL of medium were seeded into each well of a 96-well plate and incubated with various concentrations of TFM derivatives for 48 h. Following incubation, the amoebae were washed with 100 μL of pre-warmed Opti-MEM® I (Invitrogen, Carlsbad, CA) and viable cells were counted using Cell Proliferation Reagent WST-1 (Roche Diagnostics, Mannheim, Germany). Cytotoxicity against mammalian cells was examined as described above except that 1×10^4 CHO cells were cultivated in 280 μL of F-12 medium (Invitrogen) under 5% CO_2 at 37 °C.

2.4. Assay for L-methionine γ-lyase activity

Recombinant MGL1 (3 μg) or MGL2 (1.2 μg) (final concentrations 15 μg/mL and 6 μg/mL, respectively) [5] was incubated with 1 mM TFM, anilide (TFM-01) or benzylamide (TFM-02) in 200 μL of 100 mM sodium phosphate buffer (pH 7.2) containing 20 μM pyridoxal-5′-phosphate (PLP) and 2.5 mM 5,5′-dithiobis(2-nitrobenzoic acid) (Sigma, St Louis, MO) at 37 °C. Released thiols were measured as described previously [9].

2.5. Degradation of trifluoromethionine derivatives in amoebic cell lysate determined by capillary electrophoresis with electrospray ionisation time-of-flight mass spectrometry (CE-TOFMS)

Approximately 3×10^6 trophozoites were lysed with 450 μL of 10 mM HEPES (pH 7.5) containing 1 μM PLP and 0.05% Tween 20. The filtrated supernatant (50 μg) was incubated with 2 mM TFM-01, OB-01 (see Supplementary Fig. 1) or dimethyl sulphoxide (DMSO) at 37 °C for 2 h. The reaction was terminated by adding 10 times volume of methanol. TFM and 2-oxobutyrate were quantified by CE-TOFMS [11] in cationic and anionic mode, respectively, under conditions described previously [11]. TFM and sodium 2-oxobutyrate were used as standards.

2.6. Evaluation of the amoebicidal activity of trifluoromethionine derivatives using a hamster liver abscess model

Approximately 1×10^6 trophozoites were injected into the left lobe of the liver of 2–3-week-old Syrian hamsters (mean ± standard error body weight, 39.9 ± 0.56 g). TFM or its derivatives dissolved in DMSO were administered either subcutaneously (0.1 mL, 0.2 μmol/animal) or orally through a stomach catheter (0.5 mL, 0.2–1.0 μmol/animal) at 24 h after infection. Animals were sacrificed 6 days post infection and the liver and abscesses were dissected and weighed separately.

3. Results and discussion

The in vitro cytotoxicities of TFM, 15 TFM derivatives and 4 control compounds lacking fluorine were evaluated by measuring their 50% inhibitory concentration (IC_{50}) values against *E. histolytica* trophozoites (Table 1). Whilst TFM showed an IC_{50} of 7.34 μM, the derivatives TFM-01 and TFM-02 had IC_{50} values of 2.22–2.28 μM. Three difluoroanilide compounds [2,3-difluoroanilide (TFM-03), 2,6-difluoroanilide (TFM-04) and 2,5-difluoroanilide (TFM-05)] also had a comparable 2.5–3.0-fold reduction in their IC_{50} values compared with TFM. Three derivatives with 2,5- and 3,4-dimethoxyanilide (TFM-07 and TFM-08) or 3,4,5-trimethoxyanilide (TFM-09) modification had a further 2-fold improvement in their IC_{50} values. These values are 1.6–4.3-fold lower than metronidazole (mean ± standard deviation in triplicate, 4.76 μM ± 0.22). In contrast, compounds containing additional functional groups on the phenyl ring of TFM-01 [2-methyl-4-chloroanilide (TFM-10), 2-methoxy-4-bromoanilide (TFM-11), 2-methoxyl-4-chloro-5-methylaniline (TFM-12)] or bulkier structures such as 8-aminoquinoline (TFM-13), 5,6,7,8,-tetrahydro-1-naphthalenamine (TFM-14) and 4-bromo-naphthalenamide (TFM-15) had higher IC_{50} values compared with TFM. The IC_{50} values of TFM-10 and TFM-15 were >80 μM, indicating a loss of efficacy in these derivatives. Furthermore, structurally similar derivatives, in which the trifluoromethyl group was substituted by a methyl group (MET-01 or MET-09), failed to produce cytotoxic activity (IC_{50} >80 μM). These results indicate that the trifluoromethyl group at the C_5-carbon of TFM and its derivatives is essential for their cytotoxicity.

To determine whether α-keto acids generated by the release of trifluoromethane thiol from the TFM derivatives is responsible for their cytotoxic activity, OB-01 and OB-09, which were predicted products of TFM-01 and TFM-09, respectively, were evaluated. Neither OB-01 nor OB-09 showed cytotoxic activity (IC_{50} >80 μM). These results confirmed that the trifluoromethyl group is responsible for the cytotoxicity of TFM and its derivatives [7–9].

To assess whether TFM derivatives were selective towards *E. histolytica*, the efficacy of TFM, TFM-01 and TFM-02 against a representative mammalian cell line was examined. The IC_{50} values of TFM, TFM-01 and TFM-02 against CHO cells were more than 100-times higher than for *E. histolytica* (709 ± 172, 982 ± 174 and 878 ± 149 μM, respectively), whilst those of difluoroanilide and dimethoxyanilide derivatives were higher or slightly lower (>1 mM and 554 ± 94 μM, respectively). It was also previously reported that a high concentration of TFM (100 μg/mL, corresponding to 493 μM) inhibited the growth of mouse myeloma cells [8]. Taken together, TFM and its derivatives have good selectivity toward *E. histolytica*.

To determine whether the observed increase in the cytotoxic effects of the amidated TFM derivatives compared with TFM was due to their higher degradation efficiencies by MGL, time kinetics of the degradation of TFM, TFM-01 and TFM-02 by two recombinant MGL proteins (MGL1 and MGL2) were investigated [5]. Trifluoromethane thiol generated from TFM by MGL1 or MGL2 increased with incubation time (Fig. 1). Degradation of TFM by MGL2 was ca. 12.5-fold faster compared with MGL1 at 10 min after incubation, which is also consistent with a previous study [5]. In contrast, decomposition of TFM-01 and TFM-02 by MGL1 and of TFM-02 by MGL2 was negligible, whilst that of TFM-01 by MGL2 was ca. 70% slower compared with TFM.

We further examined the degradation process of TFM-01 in the amoeba by directly measuring the products formed when

Please cite this article in press as: Sato D, et al. Cytotoxic effect of amide derivatives of trifluoromethionine against the enteric protozoan parasite *Entamoeba histolytica*. Int J Antimicrob Agents (2009), doi:10.1016/j.ijantimicag.2009.08.016

Table 1
Structures and IC_{50} values of TFM and its derivatives against *E. histolytica* in vitro.

Compound name	Structure	IC_{50} (μM) (mean ± S.D.)
TFM	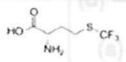	7.34 ± 0.59
TFM-01	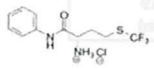	2.22* ± 0.02
TFM-02	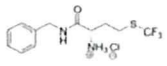	2.28* ± 0.05
TFM-03	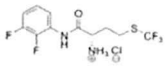	2.37* ± 0.01
TFM-04	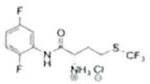	2.97* ± 0.02
TFM-05	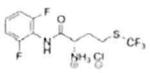	2.46* ± 0.01
TFM-06	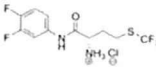	6.66* ± 0.16
TFM-07	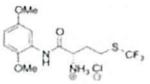	1.11* ± 0.02
TFM-08	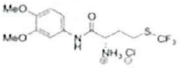	1.19* ± 0.01
TFM-09	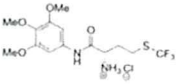	1.28* ± 0.05
TFM-10	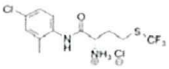	>80
TFM-11	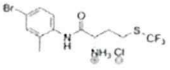	16.86* ± 0.54
TFM-12	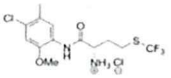	10.02 ± 0.06
TFM-13	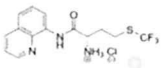	12.48 ± 0.02
TFM-14	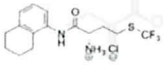	11.58 ± 0.17
TFM-15	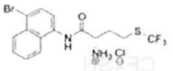	>80
MET-01	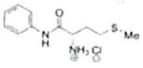	>80
MET-09	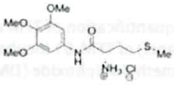	>80
OB-01	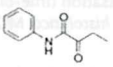	>80
OB-09	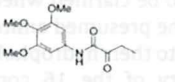	>80

Table 1 (*Continued*)

Compound name	Structure	IC_{50} (μM) (mean ± S.D.)
MNZ		4.76* ± 0.22

* *P* values <0.05 as compared to TFM.

TFM-01 was mixed with the amoebic cell lysate. TFM, TFM-01 and OB-01 were unequivocally quantified on CE-TOFMS (Fig. 2). TFM was detected in the reaction mixture at 10 min and later after the parasite lysate was mixed with TFM-01 (Fig. 2B, solid line). The concentration of TFM detected corresponded to ca. 1% of the initial TFM-01 concentration (2 mM) and did not change after further incubation. The 2-oxobutyrate detected in the reaction mixture increased during the incubation time in a linear fashion, suggestive of continuous hydrolysis and decomposition of TFM-01 that leads to 2-oxobutyrate formation (Fig. 2B, broken line). Neither TFM nor 2-oxobutyrate was detected when the cell lysate was mixed with OB-01 (data not shown). The TFM derivatives containing piperidine, pyrrolidine or morpholine linked to the C_1-carbon (without the amide bond) showed no amoebicidal activity (data not shown). These data suggest that hydrolysis of the TFM derivatives is essential for amoebicidal activity.

To confirm whether the peptidases are involved in the hydrolysis of TFM-01, the cell lysate was pre-incubated with 0.1 mM *N*-[*N*-(L-3-*trans*-carboxirane-2-carbonyl)-L-leucyl]-agmatine (E-64) or 10 mM ethylene diamine tetra-acetic acid (EDTA), respectively. These protease inhibitors reduced decomposition of TFM-01 by ca. 60% and 35%, respectively (data not shown),

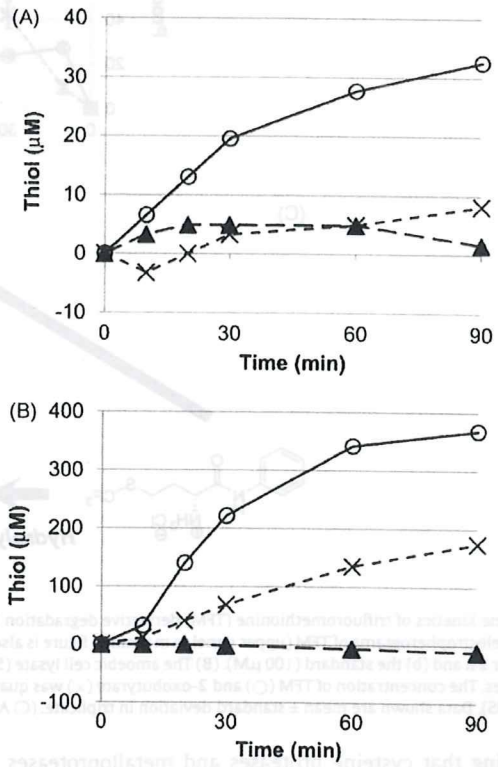

Fig. 1. Time kinetics of the degradation of trifluoromethionine (TFM) and two derivatives [anilide (TFM-01) and benzylamide (TFM-02)] by recombinant L-methionine γ-lyase (MGL). TFM (○), TFM-01 (×) and TFM-02 (▲) were incubated with (A) MGL1 or (B) MGL2 and released thiols were measured as described in Section 2.4.

Please cite this article in press as: Sato D, et al. Cytotoxic effect of amide derivatives of trifluoromethionine against the enteric protozoan parasite *Entamoeba histolytica*. Int J Antimicrob Agents (2009), doi:10.1016/j.ijantimicag.2009.08.016

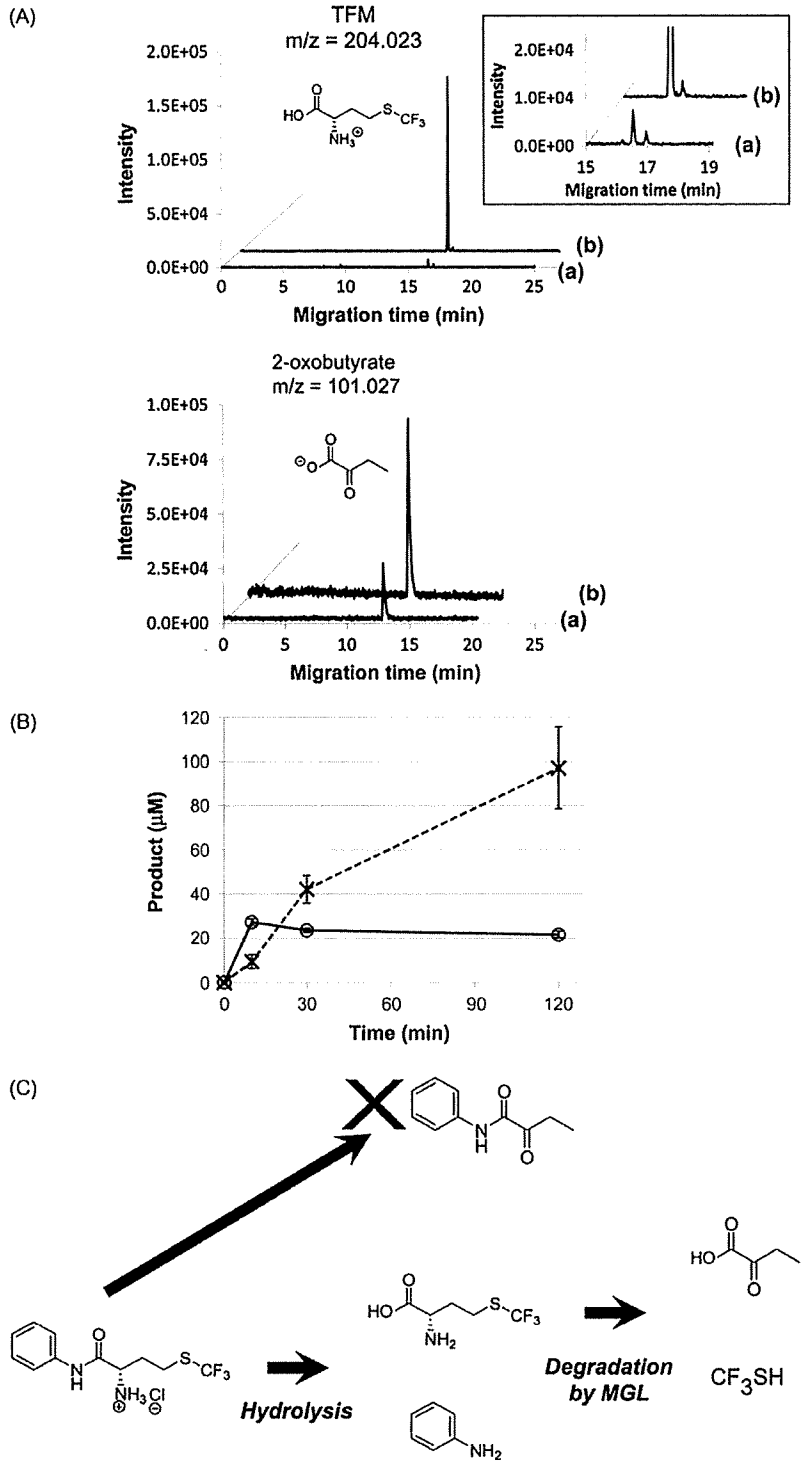

Fig. 2. Time kinetics of trifluoromethionine (TFM) derivative degradation by the amoebic cell lysate. (A) Identification and quantification of TFM and 2-oxobutyrate. Representative electropherograms of TFM (upper panel; a magnified figure is also shown in the inset) and 2-oxobutyrate (lower panel) of TFM-01 incubated with (a) the cell lysate at 37 °C for 2 h and (b) the standard (100 μM). (B) The amoebic cell lysate (50 μg) was incubated with 2 mM TFM-01 or 5% dimethyl sulphoxide (DMSO) (control) for the indicated times. The concentration of TFM (○) and 2-oxobutyrate (×) was quantified by capillary electrophoresis with electrospray ionisation time-of-flight mass spectrometry (CE-TOFMS). Data shown are mean ± standard deviation in triplicate. (C) A proposed scheme for TFM-01 degradation in *Entamoeba histolytica*. MGL, L-methionine γ-lyase.

suggesting that cysteine proteases and metalloproteases participate in the hydrolysis of TFM derivatives in *E. histolytica*. It is conceivable to assume that TFM is incorporated into the amoebae by amino acid transporter(s). It has also been reported that the parasite incorporates amino acids directly from the culture medium [12]. However, it remains to be clarified whether the TFM derivatives are incorporated via the presumed amino acid transporter(s) or by passive diffusion due to their hydrophobic nature.

The amoebicidal activity of the 16 compounds containing the trifluoromethyl group was evaluated using a hamster liver

Please cite this article in press as: Sato D, et al. Cytotoxic effect of amide derivatives of trifluoromethionine against the enteric protozoan parasite *Entamoeba histolytica*. Int J Antimicrob Agents (2009), doi:10.1016/j.ijantimicag.2009.08.016

Table 2
Amoebicidal activity of trifluoromethionine (TFM) derivatives by subcutaneous administration in a hamster amoebic liver abscess model.

Compound name	Increase in body weight (%) (mean ± S.E.)[a]	Weight of abscess (%) (mean ± S.E.)[b]	Number of animals
TFM	22.9 ± 12.8	24.5 ± 14.8	3
TFM-01	13.4 ± 0.5	29.1 ± 5.2	2
TFM-02	41.2 ± 4.3	17.9 ± 1.1	3
TFM-03	26.6 ± 2.9	32.6 ± 1.7	3
TFM-04	27.7 ± 3.4	30.3 ± 7.5	3
TFM-05	25.1 ± 2.8	15.4 ± 5.1	3
TFM-06	45.8 ± 10.6	17.7 ± 0.8	3
TFM-07	30.9 ± 2.6	15.3 ± 5.6	2
TFM-08	19.1 ± 7.2	0.2 ± 0.2	3
TFM-09	4.3 ± 4.3	8.2 ± 7.9	3
TFM-10	7.9 ± 7.9	0.2 ± 0.1	3
TFM-11	0.4 ± 0.2	19.4 ± 5.6	3
TFM-12	0.2 ± 0.2	3.2 ± 1.5	3
TFM-13	26.7 ± 13.6	5.4 ± 5.2	3
TFM-14	24.6 ± 6.3	5.6 ± 5.6	3
TFM-15	3.5 ± 0.8	0.0 ± 0.0	3
Control[c]	26.5 ± 9.0	39.7 ± 1.8	3

[a] Percentage increase in body weight between Days 0 and 6.
[b] Percentage of the abscess relative to the weight of the liver.
[c] DMSO (100 μL/head).

abscess model (Table 2). Trophozoites were directly injected into the liver and 24 h later 0.2 μmol of TFM or its derivatives were subcutaneously injected into the hamsters. Two difluoroanilide derivatives (TFM-04 and TFM-05), one dimethoxyanilide (TFM-07) and 5,6,7,8-tetrahydro-1-naphthylamide compound (TFM-14) exhibited antiamoebic effects comparable with that of TFM. All the other compounds except for TFM-06, TFM-09, TFM-11 and TFM-15 also showed comparable or slightly lower efficacy compared with TFM. It is also worth noting that the hamsters treated with TFM-04, TFM-07 or TFM-14 gained more weight compared with the other effective compounds.

Next we evaluated the in vivo efficacy of TFM-14, which showed the highest efficacy by subcutaneous administration, and TFM via oral administration (Table 3). Single oral administration of TFM at 2.54 mg/kg (0.5 μmol/animal equivalent) completely prevented liver abscess formation; TFM-14 had comparable or slightly lower potency compared with TFM [100% cure with 9.22 mg/kg (1.0 μmol/animal equivalent)]. Pargal et al. [13] showed that only 19 of 29 animals receiving 100 mg/kg (ca. 30 μmol/animal) oral metronidazole were cured of amoebic liver abscesses. Although we may not be able to compare directly their data [13] with ours because of subtle differences in experimental conditions, TFM and TFM-14 are likely to be more effective in preventing the formation of amoebic liver abscesses than metronidazole in the hamster model.

Table 3
Amoebicidal activity of trifluoromethionine (TFM) derivatives by oral administration in a hamster amoebic liver abscess model.

Compound name	Dose (mg/kg)	Increase in body weight (%) (mean ± S.E.)[a]	Weight of abscess (%) (mean ± S.E.)[b]	Number of animals
TFM	1.02	35.1 ± 2.1	7.8 ± 5.9	3
	2.54	27.6 ± 4.5	0.0 ± 0.0	3
	3.56	34.5 ± 2.2	1.7 ± 1.4	3
	5.08	27.7 ± 5.9	0.0 ± 0.0	3
TFM-14	1.84	26.3 ± 3.2	30.2 ± 1.7	3
	4.61	23.3 ± 8.3	11.3 ± 9.2	3
	6.45	22.4 ± 2.9	3.9 ± 2.5	3
	9.22	33.9 ± 3.7	0.0 ± 0.0	3
Control[c]		5.0 ± 0.9	47.6 ± 0.0	2

[a] Percentage increase in body weight between Days 0 and 6.
[b] Percentage of the abscess relative to the weight of the liver.
[c] DMSO (100 μL/head).

We have previously shown that the carbonothionic difluoride derived from TFM degradation by MGL non-specifically cross-links the primary amino group of MGL and other proteins in vitro and is responsible for the cytotoxicity of TFM [5]. Since the target of carbonothionic difluoride is non-specific and is not limited to the targets of 5-nitroimidazoles, such as pyruvate:ferredoxin oxidoreductase, thioredoxin reductase and nitroreductase [14–16], TFM and its derivatives are expected to be effective against 5′-nitroimidazole-resistant *E. histolytica* [17], *T. vaginalis* [18], periodontal bacteria and *Citrobacter freundii*.

Acknowledgments

The authors thank Rumiko Kosugi (Department of Parasitology, Gunma University Graduate School of Medicine, Gunma, Japan) for technical assistance. They also thank Mr Yuji Kakazu and Mr Akiyoshi Hirayama (Institute for Advanced Biosciences, Keio University, Yamagata, Japan) for technical help with mass spectrometry.

Funding: This work was supported by a Grant-in-Aid for Scientific Research from the Ministry of Education, Culture, Sports, Science and Technology of Japan to DS (20590429) and TN (18GS0314, 18050006 and 18073001), a grant for research on emerging and re-emerging infectious diseases from the Ministry of Health, Labour and Welfare of Japan, and a grant for research to promote the development of anti-AIDS pharmaceuticals from the Japan Health Sciences Foundation to TN.

Competing interests: None declared.

Ethical approval: Not required.

Appendix A. Supplementary data

Supplementary data associated with this article can be found, in the online version, at doi:10.1016/j.ijantimicag.2009.08.016.

References

[1] Ali V, Nozaki T. Current therapeutics, their problems, and sulfur-containing-amino-acid metabolism as a novel target against infections by "amitochondriate" protozoan parasites. Clin Microbiol Rev 2007;20:164–87.
[2] Freeman CD, Klutman NE, Lamp KC. Metronidazole. A therapeutic review and update. Drugs 1997;54:679–708.
[3] Wassmann C, Hellberg A, Tannich E, Bruchhaus I. Metronidazole resistance in the protozoan parasite *Entamoeba histolytica* is associated with increased expression of iron-containing superoxide dismutase and peroxiredoxin and decreased expression of ferredoxin 1 and flavin reductase. J Biol Chem 1999;274:26051–6.
[4] Tanaka H, Esaki N, Soda K. A versatile bacterial enzyme: L-methionine γ-lyase. Enzyme Microb Technol 1985;7:530–7.
[5] Sato D, Yamagata W, Harada S, Nozaki T. Kinetic characterization of methionine γ-lyases from the enteric protozoan parasite *Entamoeba histolytica* against physiological substrates and trifluoromethionine, a promising lead compound against amoebiasis. FEBS J 2008;275:548–60.
[6] Zygmunt WA, Tavormina PA. DL-*S*-Trifluoromethylhomocysteine, a novel inhibitor of microbial growth. Can J Microbiol 1966;12:143–8.
[7] Yoshimura M, Nakano Y, Koga T. L-Methionine-γ-lyase, as a target to inhibit malodorous bacterial growth by trifluoromethionine. Biochem Biophys Res Commun 2002;292:964–8.
[8] Coombs GH, Mottram JC. Trifluoromethionine, a prodrug designed against methionine γ-lyase-containing pathogens, has efficacy in vitro and in vivo against *Trichomonas vaginalis*. Antimicrob Agents Chemother 2001;45:1743–5.
[9] Tokoro M, Asai T, Kobayashi S, Takeuchi T, Nozaki T. Identification and characterization of two isoenzymes of methionine γ-lyase from *Entamoeba histolytica*: a key enzyme of sulfur-amino acid degradation in an anaerobic parasitic protist that lacks forward and reverse trans-sulfuration pathways. J Biol Chem 2003;278:42717–27.
[10] Clark CG, Diamond LS. Methods for cultivation of luminal parasitic protists of clinical importance. Clin Microbiol Rev 2002;15:329–41.
[11] Hirayama A, Kami K, Sugimoto M, Sugawara M, Toki N, Onozuka H, et al. Quantitative metabolome profiling of colon and stomach cancer microenvironment by capillary electrophoresis time-of-flight mass spectrometry. Cancer Res 2009;69:4918–25.
[12] Zuo X, Coombs GH. Amino acid consumption by the parasitic, amoeboid protists *Entamoeba histolytica* and *E. invadens*. FEMS Microbiol Lett 1995;130:253–8.

Please cite this article in press as: Sato D, et al. Cytotoxic effect of amide derivatives of trifluoromethionine against the enteric protozoan parasite *Entamoeba histolytica*. Int J Antimicrob Agents (2009), doi:10.1016/j.ijantimicag.2009.08.016

[13] Pargal A, Rao C, Bhopale KK, Pradhan KS, Masani KB, Kaul C. Comparative pharmacokinetics and amoebicidal activity of metronidazole and satranidazole in the golden hamster, *Mesocricetus auratus*. J Antimicrob Chemother 1993;32:483–9.
[14] Leitsch D, Kolarich D, Wilson IB, Altmann F, Duchêne M. Nitroimidazole action in *Entamoeba histolytica*: a central role for thioredoxin reductase. PLoS Biol 2007;5:e211.
[15] Pal D, Banerjee S, Cui J, Schwartz A, Ghosh SK, Samuelson J. *Giardia*, *Entamoeba*, and *Trichomonas* enzymes activate metronidazole (nitroreductases) and inactivate metronidazole (nitroimidazole reductases). Antimicrob Agents Chemother 2009;53:458–64.
[16] Samuelson J. Why metronidazole is active against both bacteria and parasites. Antimicrob Agents Chemother 1999;43:1533–41.
[17] Samarawickrema NA, Brown DM, Upcroft JA, Thammapalerd N, Upcroft P. Involvement of superoxide dismutase and pyruvate:ferredoxin oxidoreductase in mechanisms of metronidazole resistance in *Entamoeba histolytica*. J Antimicrob Chemother 1997;40:833–40.
[18] Upcroft JA, Upcroft P. Drug susceptibility testing of anaerobic protozoa. Antimicrob Agents Chemother 2001;45:1810–4.

Please cite this article in press as: Sato D, et al. Cytotoxic effect of amide derivatives of trifluoromethionine against the enteric protozoan parasite *Entamoeba histolytica*. Int J Antimicrob Agents (2009), doi:10.1016/j.ijantimicag.2009.08.016

Parasitology International 59 (2010) 75–81

Contents lists available at ScienceDirect

Parasitology International

journal homepage: www.elsevier.com/locate/parint

Identification of an avirulent *Entamoeba histolytica* strain with unique tRNA-linked short tandem repeat markers

Aleyla Escueta-de Cadiz [a,b], Seiki Kobayashi [c], Tsutomu Takeuchi [c], Hiroshi Tachibana [d], Tomoyoshi Nozaki [a,*]

[a] Department of Parasitology, National Institute of Infectious Diseases, 1-23-1 Toyama, Shinjuku-ku, Tokyo 162-8640, Japan
[b] Department of Parasitology, Gunma University Graduate School of Medicine, 3-39-22 Showa-machi, Maebashi, Gunma 371-8511, Japan
[c] Department of Tropical Medicine and Parasitology, Keio University School of Medicine, 35 Shinanomachi, Shinjuku-ku, Tokyo 160-8582, Japan
[d] Department of Infectious Diseases, Tokai University School of Medicine, Isehara, Kanagawa 259-1193, Japan

ARTICLE INFO

Article history:
Received 21 July 2009
Received in revised form 29 October 2009
Accepted 29 October 2009
Available online 4 November 2009

Keywords:
Amebiasis
Short tandem repeat
tRNA
Virulence
Symptomatic
Asymptomatic

ABSTRACT

Highly polymorphic, non-coding short tandem repeats (STR) are scattered between the tRNA genes in *Entamoeba histolytica* in a unique tandemly arrayed organization. STR markers that correlate with the virulence of individual *E. histolytica* strains have recently been reported. Here we evaluated the usefulness of tRNA-linked STR loci as genetic markers in identifying virulent and avirulent strains of *E. histolytica* from 37 Japanese *E. histolytica* samples (12 diarrheic/dysenteric, 20 amebic liver abscess (ALA), and 5 asymptomatic cases). Twenty three genotypes, assigned by combining the STR sequence types from all 6 STR loci, were identified. One to 8 new STR sequence types per locus were also discovered. Genotypes found in asymptomatic isolates were highly polymorphic (4 out of 5 genotypes were unique to this group), while in symptomatic isolates, almost half of the genotypes were shared between diarrhea/dysentery and ALA. One asymptomatic isolate (KU27) showed unique STR patterns in 4 loci. This strain, though associated with the typical pathogenic zymodeme II, failed to induce amebic liver abscess by animal challenge, which suggests that inherently avirulent *E. histolytica* strains exist, that are associated with unique genotypes. Furthermore, STR genotyping and *in vivo* challenge of 2 other asymptomatic isolates (KU14 and KU26) verified the covert virulence of these strains.

1. Introduction

Amebiasis, caused by the anaerobic/microaerophilic protozoan parasite *Entamoeba histolytica*, ranges from the asymptomatic carrier state, where patients do not show any characteristic signs of infection and microscopic stool examination often reveals the dormant cyst form, to the symptomatic state, where trophozoites damage the intestinal epithelium and cause diarrhea, colitis, and dysentery. In 5–20% of the patients with intestinal symptoms, trophozoites spread to extraintestinal organs such as the liver, lungs, and brain. The amebic liver abscess is the most common form of extraintestinal amebiasis [1,2].

What determines the outcome of infection remains to be answered. It has been shown that host immune mechanisms such as cytokines and interleukins play crucial roles in preventing or delaying tissue invasion, and specific human leukocyte antigen class II alleles have been demonstrated to reduce susceptibility to amebic infection [1,3]. On the other hand, although genetic polymorphism in *E. histolytica* isolates is well established and several polymorphic markers including the serine-rich *E. histolytica* protein (SREHP), chitinase, and repeat containing loci 1–2 and 5–6 were reported [4–9], a link between a genotype and the outcome of infection has not been demonstrated until recently [10,11].

Recent disclosure of the genome sequence of *E. histolytica* HM-1: IMSS strain [12] elucidated various unique features of the genome structure of this parasite [13]. One important finding is the presence of 4500 tandemly arrayed tRNA genes. Twenty five tRNA array units contain 1 to 5 tRNA genes which are adjoined to STRs [10]. A previous study showed that a high degree of polymorphism in these tRNA-linked STRs are observed in the early branching *E. histolytica* and its non-pathogenic sibling *Entamoeba dispar* [14]. STRs are DNA sequences of about 2 to 8 base pairs that are repeated up to 40 times in a head-to-tail manner. Currently, STR typing is widely used in paternity testing and forensic cases because the number of copies of repeats varies among individuals. A recent study indicated that *E. histolytica* tRNA-linked STRs were useful to establish a correlation between the genotype of the parasite, based on the size of the PCR-amplified fragment, and the outcome of infection [10,11]. However, a correlation remains to be established clearly at the nucleotide level between the polymorphic markers and the clinical symptoms.

Abbreviation: STR, short tandem repeat.

* Corresponding author. Tel.: +81 3 5285 1111x2600; fax: +81 327 5285 1219.
E-mail address: nozaki@nih.go.jp (T. Nozaki).

1383-5769/$ – see front matter © 2009 Published by Elsevier Ireland Ltd.
doi:10.1016/j.parint.2009.10.010

Furthermore, the potential of these tRNA-linked STRs as a marker for avirulence is not well studied.

In Japan, amebiasis is usually seen within restricted social populations such as the mentally handicapped and men who have sex with men (MSM) [7,8,15]. Epidemiological data show that the number of cases has increased from 2003 to 2007, and a higher number of cases are now also seen among female sexual workers [16]. We previously showed that extensive genetic polymorphism at SREHP, chitinase, and 2 tRNA-linked STRs (loci 1–2 and 5–6) exist in Japanese *E. histolytica* strains isolated from patients who have no history of traveling abroad [7,8]. In this study, the usefulness of 6 tRNA-linked STR loci as genetic markers has been evaluated in 37 Japanese *E. histolytica* samples, to differentiate the genotypes associated with severe or asymptomatic cases of amebiasis, although the conclusions drawn from this study may be restricted to the geographic origins where these isolates were derived from. Furthermore, we also described a unique genotype and 4 STR types, which can be used to identify potentially avirulent strains of *E. histolytica*.

2. Materials and methods

2.1. Clinical samples and cultivation

A total of 37 Japanese *E. histolytica* samples (Table 1) were included in this study (12 diarrheic/dysenteric, 20 amebic liver abscess, and 5 asymptomatic cases). Fifteen isolates which were previously described [7,8], were collected from mentally handicapped and MSM patients. Since the genotypes of isolates obtained from the mentally handicapped patients were identical within each institution [7,8], only 3 representative isolates (KU14, 26, and 27) were chosen. These isolates were recovered from liquid nitrogen and cultured either in xenic condition using Robinson's medium [17] or in monoxenic condition using yeast extract–iron–maltose–dihydroxyacetone-serum (YIMDHA-S) medium supplemented with *Crithidia fasciculata* [18,19]. Five new clinical isolates also maintained in YIMDHA-S, were obtained from Keio University School of Medicine. DNA samples was also extracted from 17 liver abscess specimens.

2.2. Polymerase chain reaction (PCR) and DNA sequencing

Total DNA from the xenic and monoxenic cultures was extracted using QIAamp DNA stool minikit (Qiagen, Tokyo, Japan), whereas the DNAs from ALA patients were extracted directly from abscess samples using the conventional methods as previously described [20]. The STR fragments were amplified using 6 *E. histolytica*-specific tRNA-linked STR primers (DA-H, AL-H, NK2-H, RR-H, SQ-H, and S^{TGA}D-H) under the conditions previously described [21]. The amplified PCR products were separated using 1.5% agarose gel (Takara, Japan) and purified using phenol/chloroform and ethanol precipitation. Sequence analysis was performed using the forward or reverse *E. histolytica*-specific tRNA-linked STR primers [21] and BigDye® Terminator v.3.1 cycle sequencing kit (Applied Biosystems, Foster City, CA). An illustra MicroSpin G-50 column (GE Healthcare, UK) was used for purifying labeled DNA from unincorporated labeled nucleotides. Sequencing was performed on an ABI PRISM 310 Genetic Analyzer. Nucleotide sequences were analyzed using the Tandem Repeats Finder software to identify the STRs [22]. Newly identified STR patterns discovered in Japanese *E. histolytica* samples were submitted to GenBank/EMBL/DDBJ database with accession numbers AB457150–AB457168.

2.3. Animal challenge with clinical isolates

Representative asymptomatic isolates (KU14, KU26 and KU27) from 3 mental institutions and the HM-1:IMSS clone 6 (HM-1) strain used as a positive control, were included in this experiment. The clinical isolates were cultured monoxenically in YIMDHA-S medium supplemented with *C. fasciculata*, while HM-1 was axenically maintained in a BI-S-33 medium. Approximately 1×10^6 trophozoites of KU14, KU26, and HM-1, harvested at the late logarithmic phase of growth, were suspended in phosphate buffer saline and directly inoculated into the left liver lobe of 3–4 week-old Syrian golden hamsters (40–50 g; 5 hamsters/strain), while $1–2 \times 10^6$ trophozoites were used for KU27. After 6 days of infection, the hamsters were sacrificed and the liver and amebic liver abscesses were dissected and weighed. The hamsters used in the experiment were not tested for antibodies against *E. histolytica*, as antibody production is not observed at 6 days of infection (S. Kobayashi, unpublished).

Table 1
Background of the Japanese *E. histolytica* samples used in this study.

No.	Isolate[a]	Clinical diagnosis	Isolation		DNA origin
			Location	Date	
1	KU 5	Asymptomatic	Tokyo	Nov 1988	Monoxenic
2	KU 14	Asymptomatic	Okayama (Institution)	Nov 1999	Xenic
3	KU 26	Asymptomatic	Shizuoka (Institution)	Sept 2000	Monoxenic
4	KU 27	Asymptomatic	Shizuoka (Institution)	Jan 2001	Xenic
5	KU 31	Asymptomatic	Tokyo	March 2001	Xenic
6	KU 1	Diarrhea	Tokyo	July 1994	Xenic
7	KU 2	Diarrhea	Tokyo	Dec 1988	Monoxenic
8	KU 3	Diarrhea	Kyoto	Sept 1988	Monoxenic
9	KU 10	Diarrhea	Tokyo	Oct 1991	Xenic
10	KU 15	Diarrhea	Tokyo	Sept 1994	Xenic
11	KU 16	Diarrhea	Tokyo	May 1993	Xenic
12	KU 23	Diarrhea	Tokyo	Feb 2000	Xenic
13	KU 32	Diarrhea	Tokyo	June 2001	Xenic
14	KU 45	Diarrhea	Chiba	April 2004	Monoxenic
15	KU 46[b]	Diarrhea	Shizuoka	April 2004	Monoxenic
16	KU 47[c]	Diarrhea	Tokyo	April 2004	Monoxenic
17	KU 50	Diarrhea	Tokyo	March 2007	Monoxenic
18	KU 8	ALA	Tokyo	May 1995	Xenic
19	KU 11	ALA	Tokyo	Feb 1994	Xenic
20	KU 48	ALA	Tokyo	May 2006	Monoxenic
21	C726	ALA	Chiba	July 2006	Abscess
22	ALA-1	ALA	Kanagawa	July 1991	Abscess
23	ALA-2	ALA	Tokyo	Nov 1990	Abscess
24	ALA-3	ALA	Ibaraki	Sept 1991	Abscess
25	ALA-4	ALA	Tokyo	Feb 1985	Abscess
26	ALA-5	ALA	Tokyo	Feb 1985	Abscess
27	ALA-6	ALA	Tokyo (Peru?)[d]	Feb 1985	Abscess
28	ALA-7	ALA	Kanagawa	March 1991	Abscess
29	ALA-8	ALA	Kagawa (Europe? Africa?)[d]	March 1991	Abscess
30	ALA-9	ALA	Ehime	Dec 1991	Abscess
31	ALA-10	ALA	Tokyo	March 1993	Abscess
32	ALA-12	ALA	Tokyo	Sept 1993	Abscess
33	ALA-13	ALA	Kanagawa	Oct 1994	Abscess
34	ALA-14	ALA	Kanagawa	June 1995	Abscess
35	ALA-15	ALA	Tokyo	April 1997	Abscess
36	ALA-16	ALA	Kanagawa	Feb 1998	Abscess
37	ALA-17	ALA	Kanagawa	June 1999	Abscess

[a] Samples 1–13, 18, 19, and 22–30 were used in previous studies (refs. [7,8,20]).
[b] Metronidazole resistant.
[c] HIV positive.
[d] Possible place of infection.

2.4. Statistical analyses

Fischer's exact test was used to evaluate the significance of correlations between the STRs and the genotypes among the different groups of infection outcomes. The mean, standard deviation and *p*-values were calculated using Student's *t*-test to determine the average percentage of abscess per liver.

3. Results and discussion

3.1. STR polymorphisms in the length and nucleotide sequences

We observed that isolates with identical PCR size-based STR types displayed distinct nucleotide sequences. We thus examined the tRNA-linked STRs of 37 Japanese *E. histolytica* samples by direct sequencing since nucleotide sequence-based differentiation of STR types is essential for high resolution typing of clinical isolates [7,8,14]. Fig. 1 shows the agarose gel pattern of 8 representative isolates in 6 loci. Variations in fragment lengths were discernible for loci N-K2, R-R, and S^{TGA}-D, but were obscure for D-A, A-L, and S-Q. Direct sequencing of the amplified STR fragments clarified this obscurity, as previously shown [14]. The STRs amplified from the samples revealed 9 STR variations in the A-L locus, 8 in N-K2, 6 in D-A and R-R loci, and 5 in S^{TGA}-D and S-Q loci (Fig. 2). Uniformity in length and sequence pattern was observed in D-A (Fig. 1A, lanes 4–8; Fig. 2A, 5DA), A-L (Fig. 1B, lanes 4, and 6–8; Fig. 2B, 4AL), and N-K2 loci (Fig. 1C, lanes 4, 7, and 11; Fig. 2C, 10NK). Although the size of the amplified products was similar in the R–R (Fig. 1D, lanes 5 and 9–11) and SQ loci (Fig. 1F, lanes 4–8 and 11), their corresponding nucleotide sequences were often distinct (Fig. 2D, 2RR/5RR; Fig. 2F, 4SQ/J4SQ). All STR types in the S^{TGA}-D locus were diverse both in length and sequence pattern (Fig. 2E). Newly identified sequences have been deposited to GenBank/EMBL/DDBJ database with accession numbers AB457150–AB457168.

3.2. STR types and genotypes of the Japanese E. histolytica strains

A genotype was assigned by combining the STR sequence types obtained from 6 STR loci and a total of 23 genotypes were identified (Table 2 and Fig. 2). The STRs that had been reported previously [14,23] or personally communicated by Dr. C. Graham Clark, London School of Hygiene and Tropical Medicine, were named according to his nomenclature, and newly identified sequence types and genotypes were assigned alphanumerical codes beginning with the letter "J" to indicate their Japanese origin.

3.2.1. Asymptomatic isolates

Of the 5 genotypes assigned to the asymptomatic group, 4 (J2 to J5) were unique to the group. Genotype J1 (KU5) was shared with the symptomatic isolates, while genotype J5 (KU31) was also similar (identical for 5 of 6 loci) to those of two ALA isolates (ALA-7 and ALA-12). KU5 and KU31 were obtained from MSM patients visiting an outpatient clinic, where they were clinically diagnosed as asymptomatic cases but were serologically positive [8]. This suggests that despite the

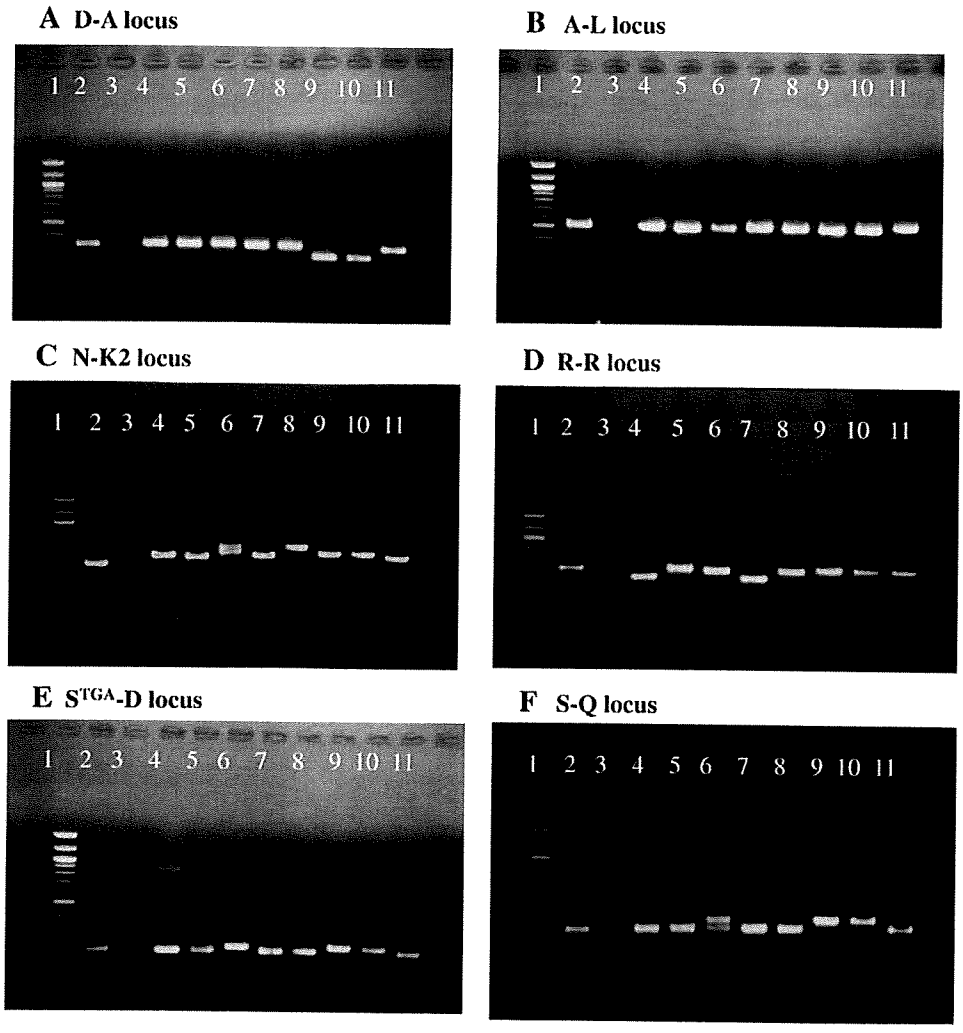

Fig. 1. Fragment length polymorphisms of 8 representative isolates in 6 tRNA-linked STR arrays. Lane 1 corresponds to the 100 bp DNA marker. Lanes 2 and 3 correspond to the reference HM-1:IMSS strain and "no template" negative control, respectively. Lanes 4 and 5 correspond to asymptomatic isolates KU5 and KU14; lanes 6–9 and 11 are isolates KU2, KU3, KU46, KU45, and KU47 from diarrheic patients; lane 10 is KU48 isolate from an ALA case. The number of the STR repeats affects variation in the size of the whole fragment that contains both non-repeat and repeat regions.

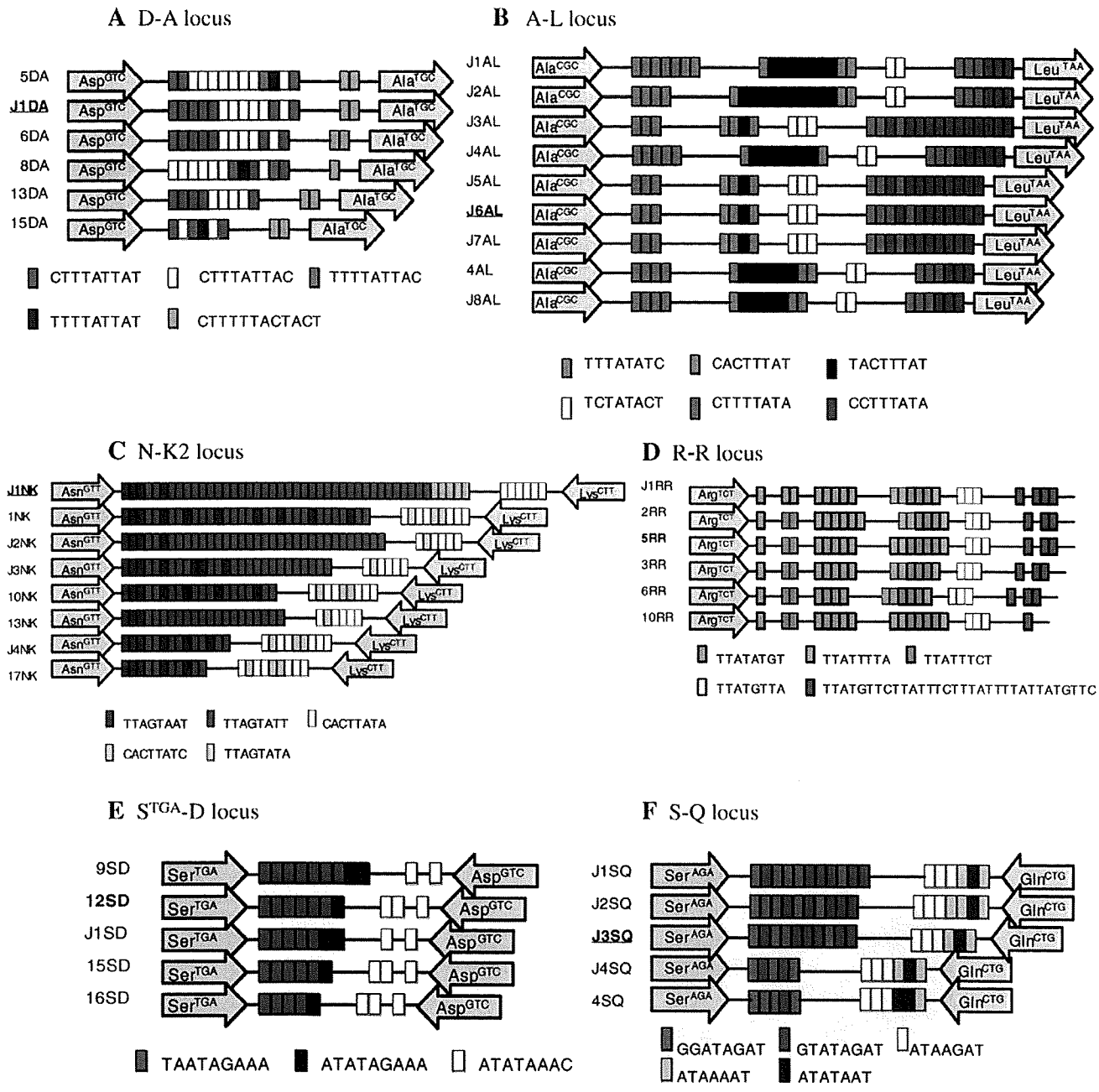

Fig. 2. Schematic representation of STR types of each loci based on the nucleotide sequence of isolates found in this study. tRNA genes and STRs are depicted in arrows and rectangles, respectively, while non-tRNA, non-STR regions are shown in lines. The 6 STR sequence types for isolate KU27 are shown in bold and the 4 STR sequence types that are unique to this isolate are underlined. The schematic diagrams of the D-A, A-L and S-Q loci were personally communicated by Dr. C. Graham Clark.

absence of symptoms invasion could be present. This premise is supported by reports of amebic colitis diagnosed through colonoscopy in asymptomatic homosexual and heterosexual Japanese patients. These patients had no gastrointestinal symptoms but had minute intestinal ulcerations containing *E. histolytica* trophozoites [24,25], which indicates that certain strains might not elicit symptoms even after tissue invasion. Thus, STR type-based genotyping may help in identifying such occult cases among asymptomatic patients.

The STR patterns of genotypes J2 and J3 (KU14 and KU26) were distinct from those in the symptomatic groups in 2 loci, while the STR patterns of the 4 remaining loci overlapped with the symptomatic groups. In contrast, the STR patterns of 4 loci were unique in genotype J4 (KU27). The unique features of the STR types of genotype J4 are discussed below. Genotypes J2 to J4 were seen among isolates from different mental institutions. We chose only one representative asymptomatic isolate each from institutions in the present study, because our previous genotyping of loci 1–2, 5–6, SREHP, and chitinase [7,8] of asymptomatic isolates showed that the genotypes of the isolates from a single institution were identical. However, the better resolution power of the STR-based typing using 6 loci may reveal heterogeneity of the genotypes among isolates from a single institution.

Table 2
Genotypes of Japanese *E. histolytica* samples using tRNA-linked STR markers.

Outcome of infection	Sample no	Sequence type[a]						Genotype[b]
		D-A	A-L	N-K2	R-R	S^{TGA}-D	S-Q	
Asymptomatic	KU5	5DA	4AL	10NK	10RR	15SD	4SQ	J1
	KU14	5DA	J5AL	***13NK***	2RR	***J1SD***	4SQ	J2
	KU26	***13DA***	***J7AL***	10NK	3RR	15SD	4SQ	J3
	KU27[c]	***J1DA***	***J6AL***	***J1NK***	**5RR**	**12SD**	***J3SQ***	J4
	KU31	8DA	J8AL	10NK	5RR	12SD	J2SQ	J5
Diarrhea	KU3	5DA	4AL	10NK	10RR	15SD	4SQ	J1
	KU1	5DA	J5AL	***J2NK***	2RR	***16SD***	4SQ	J6
	KU2	5DA	4AL	J3NK	6RR	9SD	***J4SQ***	J7
	KU10	5DA	4AL	1NK	6RR	15SD	4SQ	J8
	KU46	5DA	4AL	1NK	6RR	15SD	4SQ	J8
	KU15	15DA	J8AL	J3NK	5RR	12SD	J1SQ	J9
	KU16	6DA	***J4AL***	J3NK	6RR	9SD	J1SQ	J10
	KU23	6DA	***J1AL***	J4NK	3RR	15SD	4SQ	J11
	KU32	8DA	J8AL	J3NK	5RR	9SD	J1SQ	J12
	KU45	15DA	J8AL	J3NK	5RR	9SD	J1SQ	J13
	KU47	8DA	J2AL	10NK	5RR	15SD	4SQ	J14
	KU50	15DA	J8AL	J3NK	5RR	9SD	4SQ	J15
Amebic liver abscess	ALA-3	5DA	4AL	10NK	10RR	15SD	4SQ	J1
	ALA-10	5DA	4AL	10NK	10RR	15SD	4SQ	J1
	ALA-1	5DA	4AL	1NK	6RR	15SD	4SQ	J8
	ALA-2	5DA	4AL	1NK	6RR	15SD	4SQ	J8
	ALA-5	5DA	4AL	1NK	6RR	15SD	4SQ	J8
	ALA-6	5DA	4AL	1NK	6RR	15SD	4SQ	J8
	C726	15DA	J8AL	J3NK	5RR	9SD	J1SQ	J13
	ALA-4	15DA	J8AL	J3NK	5RR	9SD	J1SQ	J13
	ALA-14	15DA	J8AL	J3NK	5RR	9SD	J1SQ	J13
	KU8	15DA	J8AL	J3NK	5RR	9SD	J1SQ	J13
	KU48	15DA	J8AL	J3NK	5RR	9SD	J1SQ	J13
	ALA-13	5DA	4AL	10NK	10RR	15SD	J2SQ	J16
	ALA-8	6DA	4AL	J3NK	5RR	9SD	J2SQ	J17
	ALA-9	6DA	***J3AL***	J4NK	***J1RR***	15SD	4SQ	J18
	ALA-17	6DA	***J3AL***	***17NK***	***J1RR***	15SD	4SQ	J19
	ALA-7	8DA	J2AL	10NK	5RR	12SD	J2SQ	J20
	KU11	15DA	J8AL	J3NK	6RR	15SD	4SQ	J21
	ALA-12	15DA	J8AL	10NK	5RR	12SD	J2SQ	J22
	ALA-15	15DA	J2AL	10NK	5RR	9SD	J2SQ	J23
	ALA-16	15DA	J2AL	10NK	5RR	9SD	J2SQ	J23

[a] STR sequence types unique to an individual group (i.e., asymptomatic, diarrhea, or liver abscess) are shown in bold/italics.
[b] Genotypes shared by >1 group are shown in bold and underlined (J1), double-underlined (J8), or dotted-underlined (J13).
[c] Unique STR sequence types in 4 loci of the asymptomatic KU27 isolate are shown in bold/italics/underlined; 2 non-unique STR type are shown in bold/underlined.

3.2.2. Diarrhea/dysentery and ALA samples

Of the 12 diarrhea/dysentery isolates, 8 genotypes were distinct from those found in the other groups (i.e., ALA and asymptomatic). Eight unique genotypes were also found exclusively in the ALA group (J16 to J23). Our findings reaffirm the results obtained in the previous study by Ali *et al* [11], where they identified unique genotypes linked with intestinal and extraintestinal amebiasis. The dominant genotypes among strains causing both diarrhea/dysentery and ALA were J8 and J13. Genotype J1 was seen in all groups, while J8 and J13 were also found in 4 and 5 ALA-derived isolates, respectively. The shared genotypes observed between the diarrhea/dysentery and ALA in the present study suggests an inherent limitation of STR to predict isolates that cause the two major forms of symptomatic infections.

3.3. Unique STR sequence types in 9 Japanese E. histolytica samples: possible markers in identifying virulent and avirulent strains of E. histolytica

Sixteen STR sequence types unique to individual groups (i.e., asymptomatic, diarrhea/dysentery, and ALA) were identified in 9 genotypes/samples (Table 2, Fig. 3). Twelve out of the 16 STR sequence types were unique to the Japanese *E. histolytica* samples. A half of these 16 sequence types (13DA/J1DA, J6AL/J7AL, J1NK/13NK, J1SD, and J3SQ) were uniquely found in 3 asymptomatic cases. On the other hand, types J1AL/J4AL, J2NK, 16SD, and J4SQ were identified in 4 diarrhea/dysentery isolates, and types J3AL, 17NK, and J1RR in 2 ALA samples. Although it was previously suggested that STR polymorphism cannot be directly linked to the virulence of *E. histolytica* [21], the highly polymorphic STR types in a relatively small sample size of the asymptomatic group should justify the use of these STRs in differentiating the avirulent strains from virulent strains, and eventually lead to an understanding of the reasons behind the spectrum of the virulence. However, since the number of isolates showing symptom-specific STR types was also small, these premises need to be tested further.

3.4. The unique features of STR types of the KU27 isolate

One remarkable finding in the present study is the unique STR sequence types exhibited by the KU27 isolate. This strain was isolated from an asymptomatic cyst carrier and showed distinct STR sequence types in the D-A, A-L, N-K2, and S-Q loci. It also showed unique patterns in the SREHP gene and locus 1–2 [8]. The locus 1–2 also contains internal repeats and is now termed as locus D-A [9,21]. In the present study, the insertion of one repeat unit (CTTTATTAC) in the first block of the D-A locus singled out KU27 from the rest of the samples (Fig. 2A). Base substitution and arrangement of the repeats in the fourth repeat block of the A-L locus discriminated KU27 from KU14, another asymptomatic isolate with the same STR fragment length (Fig. 2B). Variation in the number of repeats, arrangement, and base substitution in two blocks of the repeat unit of the S-Q locus differentiated KU27 from the rest of asymptomatic isolates (Fig. 2E). The STR sequence pattern of KU27 was most remarkable in the N-K2 locus, where 5 additional repeats of the TTAGTATA stretch were present (Fig. 2C), and, with 45 repeats, is also the longest STR repeats identified to date [14]. It was suggested that replication slippage during DNA replication and repair gives rise to length changes in microsatellite DNA. These mutations correspond to the unrepaired regions of DNA strands supposed to be restored by a mismatch repair system [26]. It is not known if all tRNA genes with intergenic STR regions are transcribed and whether all are functional [10,14].

3.5. Polymorphism in the in vivo virulence of E. histolytica isolates from asymptomatic cases

To support the unique nature of KU27, which belongs to the typical pathogenic zymodeme II, and to confirm whether the STRs unique to asymptomatic isolates can be used as surrogate markers for avirulence, animal challenge of HM-1 and 3 representative asymptomatic isolates (KU14, KU26, and KU27) was performed (Table 3). KU14, KU26, and HM-1 induced ALA formation, occupying about 35 to 43% of the total weight of infected livers, while no abscess was observed in hamsters infected with KU27 even after the inoculum's size was doubled. The xenically grown KU27 isolate also failed to infect the caeca of gerbils and the C3H/HeJ mice, which are known to be susceptible to intestinal *E. histolytica* infection (S. Kobayashi, unpublished data).

The weight of ALA formed by KU14 and KU26 isolates was comparable to that of the virulent reference strain HM-1 (p-value, 0.828 and 0.384, respectively; Table 3). Thus, the isolates of genotypes J2 and J3 have the capacity to induce ALA in hamsters, indicating that not all of the isolates derived from asymptomatic cases are avirulent *in vivo*. These data suggest that factors other than parasite genotype, such as the presence of bacteria, and host immune system, determine the outcome of infection, as previously suggested [1,3,27–29]. It is also possible that patients infected with J2 and J3 genotypes had a latent invasive amebic infection that was not detected at the time of study. Alternatively, STR typing may not be robust enough to predict the behavior of all isolates from asymptomatic cases, thus more studies

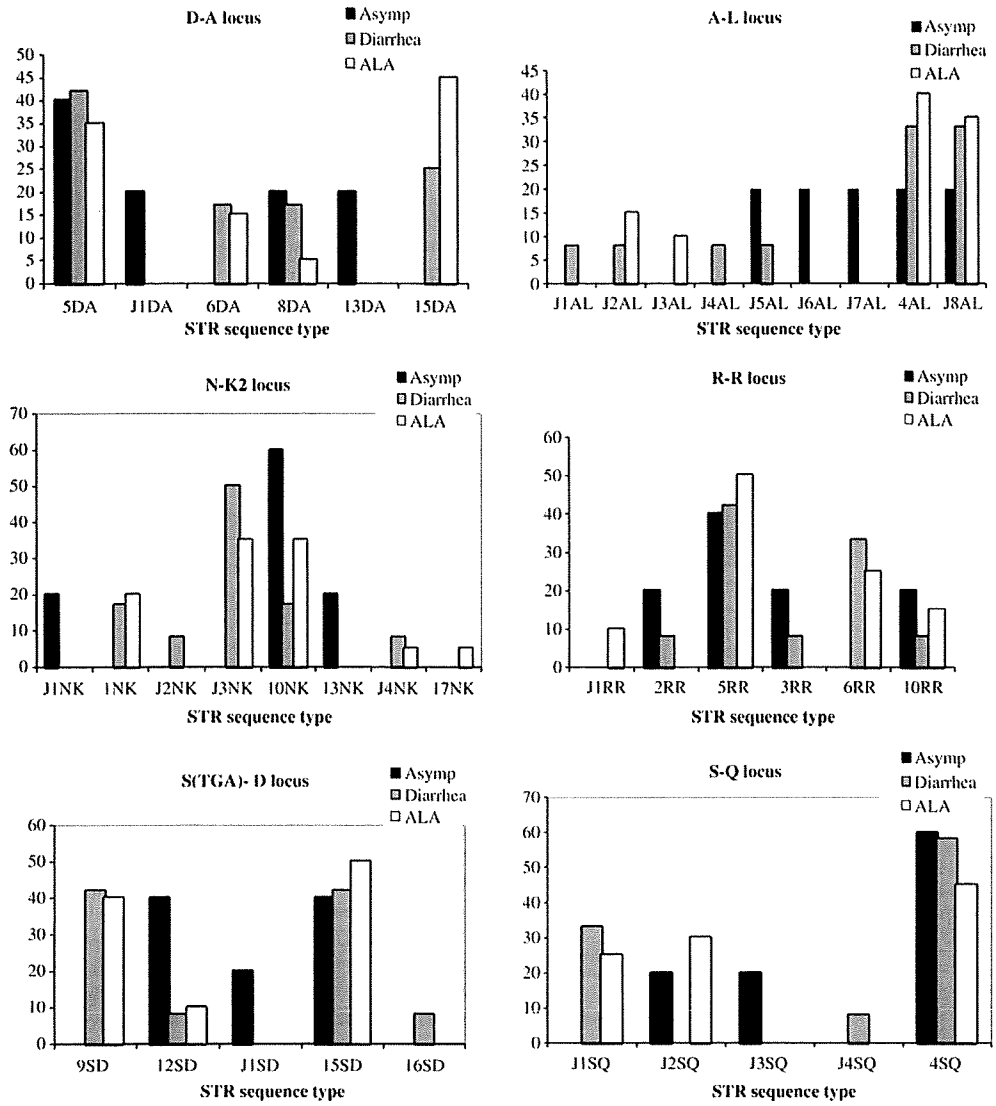

Fig. 3. Frequency distribution of the STR types among different outcomes of infections.

are needed to strengthen predictions regarding pathogenicity based on STR sequences.

3.6. The KU27 isolate represents a new avirulent strain of E. histolytica

Genotype J4 and its 4 STR types unique to KU27 are potential surrogate markers for the avirulence of an isolate. Previous microarray studies that used the non-virulent Rahman strain pinpointed specific genes whose expression are potentially linked with the avirulent phenotype [30,31]. However, it remains questionable whether the Rahman strain is avirulent because it was previously known to cause ALA in animals, although its virulence has already been attenuated [13,32]. Thus, our avirulent KU27 strain could be a good representative isolate in mining new avirulence-associated genes. In summary, our present work identified a prototype avirulent *E. histolytica* strain and its genetic markers. It needs to be further determined whether this avirulence-associated genotype is shared by other clinical isolates or unique to this strain.

Table 3
In vivo animal challenge of representative asymptomatic isolates.

Isolate	[a]Body weight on day 6 (mean ± S.E.)	Abscess weight in grams (mean ± S.E.)	Total liver weight in grams (mean ± S.E.)	Percentage (%) of abscess (mean ± S.E.)	*p*-value vs KU27	*p*-value vs HM-1
KU27	68.6 ± 2.48[b]	0 ± 0	4.12 ± 0.375	0 ± 0		<0.0001
KU26	59.0 ± 7.48	2.72 ± 0.625	6.70 ± 1.26	35.3 ± 15.2	0.0006	0.828
KU14	60.5 ± 2.31	2.92 ± 0.553	6.73 ± 0.479	43.3 ± 6.40	<0.0001	0.384
HM-1[c]	47.3 ± 2.2	2.03 ± 0.620	5.13 ± 0.301	39.7 ± 1.8	<0.0001	

[a] Average body weight (in grams) of 5 Syrian hamsters after 6 days of infection.
[b] Mean and standard deviation.
[c] Positive control.

Acknowledgments

We thank Dr. Jun Suzuki of Tokyo Metropolitan Institute of Public Health for providing C726, Drs. Haruyoshi Tomita and Yasuyoshi Ike, Gunma University Graduate Schoold of Medicine, for the use of the sequencing apparatus and technical assistance on direct sequencing of PCR fragments, and Mr. Gil M. Penuliar for careful proofreading of the manuscript. This work was supported in part by a grant for research on emerging and re-emerging infectious diseases from the Ministry of Health, Labour and Welfare of Japan to T.N., Grant-in-Aids for Scientific Research from the Ministry of Education, Culture, Sports, Science and Technology of Japan to T.N. (18GS0314, 18050006, and 18073001), and a grant for research to promote the development of anti-AIDS pharmaceuticals from the Japan Health Sciences Foundation to T.N.

References

[1] Stanley S. Amoebiasis. Lancet 2003;361:1025–34.
[2] Tanyuksel M, Petri Jr WA. Laboratory diagnosis of amebiasis. Clin Microbiol Rev 2003;16:713–29.
[3] Duggal PR, Haque R, Roy S, Mondal D, Sack RB, Farr BM, et al. Influence of human leukocyte antigen class II alleles on susceptibility to *Entamoeba histolytica* infection in Bangladeshi children. J Infect Dis 2004;189:520–6.
[4] Ali IKM, Clark CG, Petri Jr WA. Molecular epidemiology of amebiasis. Infect Genet Evol 2008;8:698–707.
[5] Ayeh-Kumi PF, Ali IKM, Lockhart LA, Gilchrist CA, Petri Jr WA, Haque R. *Entamoeba histolytica*: genetic diversity of clinical isolates from Bangladesh as demonstrated by polymorphisms in the serine-rich gene. Exp Parasitol 2001;99:80–8.
[6] Ghosh S, Frisardi M, Ramirez-Avila L, Descoteaux S, Sturm-Ramirez K, Newton-Sanchez OA, et al. Molecular epidemiology of *Entamoeba* spp evidence of a bottleneck (demographic sweep) and transcontinental spread of diploid parasites. J Clin Microbiol 2000;38:3815–21.
[7] Haghighi A, Kobayashi S, Takeuchi T, Thammapalerd N, Nozaki T. Geographic diversity of genotypes among *Entamoeba histolytica* field isolates. J Clin Microbiol 2003;41:3748–56.
[8] Haghighi A, Kobayashi S, Takeuchi T, Masuda G, Nozaki T. Remarkable genetic polymorphism among *Entamoeba histolytica* isolates from a limited geographic area. J Clin Microbiol 2002;40:4081–90.
[9] Zaki M, Meelu P, Sun W, Clark CG. Simultaneous differentiation and typing of *Entamoeba histolytica* and *Entamoeba dispar*. J Clin Microbiol 2002;40:1271–6.
[10] Clark CG, Ali IKM, Zaki MB, Loftus J, Hall N. Unique organization of tRNA genes in *Entamoeba histolytica*. Mol Biochem Parasitol 2006;146:24–9.
[11] Ali IKM, Mondal U, Roy S, Haque R, Petri Jr WA, Clark CG. Evidence for a link between parasite genotype and outcome of infection with *Entamoeba histolytica*. J Clin Microbiol 2007;45:285–9.
[12] Loftus B, Anderson I, Davies R, Alismark UCM, Samuelson J, Amedeo P, et al. The genome of the protist parasite *Entamoeba histolytica*. Nature 2005;433:865–8.
[13] Clark CG, Cecilia U, Alsmark M, Hofer M, Saito-Nakano Y, Ali V, et al. Structure and content of the *Entamoeba histolytica* genome. Adv Parasitol 2007;65:51–190.
[14] Tawari B, Ali IKM, Scott C, Quail MA, Berriman M, Hall N, et al. Patterns of evolution in the unique tRNA gene arrays of the genus *Entamoeba*. Mol Biol Evol 2008;25:187–98.
[15] Nozaki T, Kobayashi S, Takeuchi T, Haghighi A. The diversity of clinical isolates of *Entamoeba histolytica* in Japan. Arch Med Res 2005;37:276–8.
[16] Infectious Agents Surveillance Report. AmebiasisInfectious Disease Surveillance Center, National Institute of Infectious Disease; 2007. p. 103–4.
[17] Robinson GL. The laboratory diagnosis of human parasitic amoebae. Trans R Soc Trop Med Hyg 1968;62:285–94.
[18] Kobayashi S, Imai E, Haghighi A, Khalifa S, Tachibana H, Takeuchi T. Axenic cultivation of *Entamoeba dispar* in newly designed yeast extract-iron-gluconic acid-dihydroxyacetone-serum medium. J Parasitol 2005;91:1–4.
[19] Suzuki J, Kobayashi S, Murata R, Tajima H, Hashizaki F, Yanagawa Y, et al. A survey of amoebic infections and differentiation of an *Entamoeba histolytica*-like variant (JSK2004) in non-human primates by a multiplex polymerase chain reaction. J Zoo Wildl Med 2008;39:370–9.
[20] Tachibana H, Kobayashi S, Okuzawa E, Masuda G. Detection of pathogenic *Entamoeba histolytica* DNA in liver abscess fluid by polymerase chain reaction. Int J Parasitol 1992;22:1193–6.
[21] Ali IKM, Zaki M, Clark CG. Use of PCR amplification of tRNA gene-linked short tandem repeats for genotyping *Entamoeba histolytica*. J Clin Microbiol 2005;43:5842–7.
[22] Benson G. Tandem repeats finder: a program to analyze DNA sequences. Nucleic Acids Res 1999;27:573–80.
[23] Ali IKM, Solaymani-Mohammadi S, Akhter J, Roy S, Gorrini C, Calderaro A, et al. Tissue invasion by *Entamoeba histolytica:* evidence of genetic selection and/or DNA reorganization events in organ tropism. PLoS Negl Trop Dis 2008;2:e219.
[24] Okamoto M, Kawabe T, Ohata K, Togo G, Hada T, Katamoto T, et al. Amebic colitis in asymptomatic subjects with positive fecal occult blood test results: clinical features different from symptomatic cases. Am J Trop Med Hyg 2005;73:934–5.
[25] Yoshikawa I, Murata I, Yano K, Kume K, Otsuki M. Asymptomatic amebic colitis in a homosexual man. Am J Gastroenterol 1999;94:2306–8.
[26] Ellegren H. Microsatellite: simple sequences with complex evolution. Nature Rev Genet 2004;5:435–43.
[27] Haque R, Mondal D, Duggal P, Kabir M, Roy S, Farr BM, et al. *Entamoeba histolytica* infection in children and protection from subsequent amebiasis. Infect Immun 2006;38:3815–21.
[28] Padilla-Vaca F, Ankri S, Bracha R, Koole LA, Mirelman D. Down regulation of *Entamoeba histolytica* virulence by monoxenic cultivation with *Escherichia coli* O55 is related to a decrease in expression of the light (35-kilodalton) subunit of the Gal/GalNAc lectin. Infect Immun 1999;67:2096–102.
[29] Mirelman D. Ameba-bacterium relationship in amebiasis. Microbiol Rev 1987;51:272–84.
[30] Davis P, Schulze J, Stanley SJ. Transcriptomic comparison of two *Entamoeba histolytica* strains with defined virulence phenotypes identifies new virulence factor candidates and key differences in the expression patterns of cysteine proteases, lectin light chains, and calmodulin. Mol Biochem Parasitol 2007;151:118–28.
[31] MacFarlane RC, Singh U. Identification of differentially expressed genes in virulent and non-virulent *Entamoeba* species: potential implications for amebic pathogenesis. Infect Immun 2006;74:340–51.
[32] Mattern C. and Keister D. Experimental Amebiasis II Hepatic amebiasis in the newborn hamster Am J Trop Med Hyg 1977;26:403–11.

cmi_1397

Cellular Microbiology (2009) doi:10.1111/j.1462-5822.2009.01397.x

Bacterial-type oxygen detoxification and iron-sulfur cluster assembly in amoebal relict mitochondria

Barbora Maralikova,[1] Vahab Ali,[2,†] Kumiko Nakada-Tsukui,[2,3] Tomoyoshi Nozaki[2,3] Mark van der Giezen,[1,‡] Katrin Henze[4] and Jorge Tovar[1]

[1]*School of Biological Sciences, Royal Holloway University of London, Egham TW20 0EX, UK.*

[2]*Department of Parasitology, Gunma University Graduate School of Medicine, Maebashi, 371–8 511, Japan.*

[3]*Department of Parasitology, National Institute of Infectious Diseases, Tokyo 162–8640, Japan.*

[4]*Institute of Botany III, Heinrich Heine University, 40225 Düsseldorf, Germany.*

Summary

The assembly of vital reactive iron-sulfur (Fe-S) cofactors in eukaryotes is mediated by proteins inherited from the original mitochondrial endosymbiont. Uniquely among eukaryotes, however, Entamoeba and Mastigamoeba lack such mitochondrial-type Fe-S cluster assembly proteins and possess instead an analogous bacterial-type system acquired by lateral gene transfer. Here we demonstrate, using immunomicroscopy and biochemical methods, that beyond their predicted cytosolic distribution the bacterial-type Fe-S cluster assembly proteins NifS and NifU have been recruited to function within the relict mitochondrial organelles (mitosomes) of Entamoeba histolytica. Both Nif proteins are 10-fold more concentrated within mitosomes compared with their cytosolic distribution suggesting that active Fe-S protein maturation occurs in these organelles. Quantitative immunoelectron microscopy showed that amoebal mitosomes are minute but highly abundant cellular structures that occupy up to 2% of the total cell volume. In addition, protein colocalization studies allowed identification of the amoebal hydroperoxide detoxification enzyme rubrerythrin as a mitosomal protein. This protein contains functional Fe-S centres and exhibits peroxidase activity in vitro. Our findings demonstrate the role of analogous protein replacement in mitochondrial organelle evolution and suggest that the relict mitochondrial organelles of Entamoeba are important sites of metabolic activity that function in Fe-S protein-mediated oxygen detoxification.

Received 8 July, 2009; revised 13 October, 2009; accepted 15 October, 2009. *For correspondence. E-mail j.tovar@rhul.ac.uk; Tel. (+44) 1784 414159; Fax (+44) 1784 414224.
Present addresses: †Department of Biochemistry, Rajendra Memorial Research Institute of Medical Sciences, Agamkuan, Patna-800 007, India; ‡Centre for Eukaryotic Evolutionary Microbiology, School of Biosciences, University of Exeter, Exeter, EX4 4QD, UK.

Introduction

Life on earth is dependent on the activities of highly reactive Fe-S centre-containing proteins that mediate key biological functions such as electron transport, metabolic regulation, metalloenzyme catalysis and chemical sensing (Beinert *et al.*, 1997; Beinert, 2000). In bacteria such Fe-S centres are assembled via one or more of three systems of diverse molecular complexity which are known as nitrogen fixation (Nif), mobilization of sulfur and iron-sulfur cluster (Isc) systems (Lill and Kispal, 2000; Rees and Howard, 2000; Craig and Marszalek, 2002; Takahashi and Tokumoto, 2002; Frazzon and Dean, 2003; Loiseau *et al.*, 2003; Outten *et al.*, 2003; Lill and Mühlenhoff, 2008). Although variable in their molecular composition all three Fe-S cluster assembly systems rely on the enzymatic transfer of molecular sulfur from cysteine to molecular iron through the concerted action of cysteine desulfurase and of scaffold iron-binding proteins to form transient Fe-S centres, which are then transferred to their final target apoproteins in a process known as Fe-S protein maturation.

Most eukaryotic cells inherited the Isc system from the original mitochondrial endosymbiont. Genetic and biochemical studies have shown that the maturation of cytosolic and mitochondrial Fe-S proteins is dependent on Fe-S centres assembled in mitochondria and have identified Fe-S cluster assembly as the only essential biosynthetic function of this organelle (Lill and Kispal, 2000; Gerber *et al.*, 2004). Interestingly, microbial eukaryotes that lack recognizable mitochondria seem to carry out this function in mitochondrion-related organelles known as mitosomes or hydrogenosomes (Tovar *et al.*, 2003; Sutak *et al.*, 2004; Goldberg *et al.*, 2008). These organelles share a common ancestry with mitochondria and have

evolved several times independently in diverse protist and fungal lineages (Embley *et al.*, 1995; van der Giezen *et al.*, 2005a; Embley, 2006; Tovar, 2007). Given the monophyletic nature of mitochondria and the mutually exclusive distribution between mitosomes, mitochondria and hydrogenosomes, all of these organelles are considered evolutionary derivatives of the original mitochondrial endosymbiont.

The functional minimalism of mitosomes is apparent from genome surveys of mitosome-bearing organisms such as *Giardia, Entamoeba* and *Encephalitozoon* which have revealed molecular chaperonins and Fe-S cluster assembly proteins as sole common features (Katinka *et al.*, 2001; Loftus *et al.*, 2005; Morrison *et al.*, 2007). Fe-S cluster biosynthesis and Fe-S protein maturation were originally demonstrated in *Giardia* mitosomes (Tovar *et al.*, 2003) and recent evidence on the localization and functionality of microsporidial Fe-S cluster assembly proteins suggests that *Encephalitozoon cuniculi* mitosomes may also fulfil this function (Goldberg *et al.*, 2008). The essential nature of Fe-S cluster assembly in eukaryotes and the lack of evidence for additional mitosomal functions strongly suggest that retention of mitochondrial organelles may be driven by the need of *in organello* Fe-S cluster assembly and Fe-S protein maturation (Embley *et al.*, 2003; Tovar *et al.*, 2003). However, the discovery that *Entamoeba* lacks the mitochondrial-type Isc system of Fe-S cluster assembly and possesses instead a non-redundant bacterial-type Nif system acquired by lateral transfer from epsilon proteobacteria (Ali *et al.*, 2004; van der Giezen *et al.*, 2004) challenged the validity of this hypothesis. Here we report on the unusual cellular distribution of the amoebal Fe-S cluster assembly proteins NifS and NifU and show that peroxide detoxification and FeS cluster assembly are physiological functions of *Entamoeba histolytica* mitosomes.

Results

Dual distribution of amoebal NifS/NifU

Amoebas of the genera *Entamoeba* and *Mastigoamoeba* stand alone among eukaryotes in possessing bacterial-type Fe-S cluster assembly proteins instead of their canonical mitochondrial-type analogues (Ali *et al.*, 2004; van der Giezen *et al.*, 2004; Gill *et al.*, 2007). We previously demonstrated that *E. histolytica* NifS and NifU were likely acquired by lateral gene transfer from epsilon-proteobacteria and that these proteins fulfil a non-redundant functional role (Ali *et al.*, 2004; van der Giezen *et al.*, 2004). Coexpressed NifS and NifU are able to complement the growth defect of mutant *Escherichia coli* whose *isc* and *suf* operons had been removed by targeted gene deletion, demonstrating that both proteins are necessary and sufficient for the biosynthesis of Fe-S clusters under anaerobic conditions (Ali *et al.*, 2004). Purified recombinant proteins NifS and NifU expressed in bacteria were used to generate specific homologous antibodies which have been used in this study to define the cellular distribution of these proteins in parasite trophozoites.

Laser scanning confocal microscopy imaging revealed an unconventional distribution pattern for amoebal NifS and NifU. Both proteins appear distributed throughout the cytoplasm but their distribution seems uneven, with some punctate labelling that could suggest partial compartmentalization (Fig. 1A–H). Western blot analysis of trophozoite extracts separated by differential centrifugation showed that although most amoebal Nif proteins remain in the high speed supernatant (cytosol), a significant proportion of each protein appears associated with the mixed membrane fraction (MMF), which is a mixture of broken membranes and membrane-bounded organelles (Fig. 1I). Together these data suggested that *E. histolytica* Nif proteins could be both cytosolic and associated with membranous cellular structures.

NifS and NifU are enriched in mitosomes

To investigate the apparent unusual distribution of Nif proteins further we used a more refined and powerful imaging method, immunoelectron microscopy. Our initial studies focused on the identification of *Entamoeba* mitosomes using a specific antibody against the mitosomal marker protein Cpn60, a crucial control in our experiments because the Fe-S cluster biosynthetic proteins in all other eukaryotes are known to reside in mitochondrial organelles (including mitosomes and hydrogenosomes where present). Immunogold labelling of Cpn60 identified mitosomes as minute spherical structures of around 100 nm in diameter surrounded by two limiting membranes (Fig. 2A and D). Little or no cytosolic labelling was detected for this antigen, in agreement with the distribution of Cpn60 observed by confocal microscopy (León-Avila and Tovar, 2004). Interestingly, similar cellular organelles were observed by immunogold labelling of NifS and NifU. In this case, however, both antigens were also found widely distributed throughout the cytosol (Fig. 2B, C, E and F), in agreement with the distribution observed for these proteins by confocal imaging (Fig. 1). Double labelling for Cpn60 and NifS as well as Cpn60 and NifU colocalized these three antigens to the same intracellular structures (Fig. 2G and H respectively) thus demonstrating that amoebal Fe-S cluster assembly proteins have a dual cytosolic and compartmentalized distribution and that the compartments harbouring NifS and NifU are mitosomes.

Ectopic expression of NifS and NifU

In an attempt to increase the rate of Fe-S cluster assembly and Fe-S protein maturation in the parasite we generated